# APPENDIX G
# AIR INGRESS STUDY

## G.1 Background

As part of the PIRT process, the NRC panel members felt that calculations of the postulated air ingress event were needed to better inform the panel members about the potential conditions that fuel pebbles experience in a postulated air ingress event. A MELCOR model has been under development for the past few years at the INEEL to scope out the important phenomena related to air ingress events in a pebble bed reactor. These results were presented recently at a gas reactor conference [G-1]. The results showed that a significant amount of the pebble bed core would not be exposed to air. The factors, which contributed to this calculated result, include the large flow resistance between the postulated breach location and the core, the extended time for natural convection to begin, the limited oxygen available in the reactor containment, and the large amount of lower reflector graphite available for oxidation, which acts as a sink for any oxygen in the air.

The MELCOR model has been improved and now includes the effect of neutron fast fluence on the thermal conductivity of the pebble bed core and detailed modeling of the region between the reactor pressure vessel (RPV) and reactor cavity cooling system (RCCS). As a result, the analyses conducted for the PIRT panel are different than earlier scoping results. Calculations were performed for alternate scenarios that could result in varying amounts of air entering the active region of the core to determine what conditions the fuel could hypothetically experience in this event. The calculations are not intended to be a best estimate calculation of such an events in a PBR. The calculation are intended to provide realistically conservative basis for understanding the accident condition and identifying the important phenomena that could affect fuel performance and fission product transport. The calculations also aid in the understanding of the potential interactions between the system thermal hydraulics, core thermal response and oxidation behavior under a wide range of scenarios. The following eight cases were analyzed:

- Case 1: Base case.
- Case 2: Reduced effective thermal conductivity of the pebble bed core
- Case 3: Significant leak in the upper head of the reactor vessel (to investigate its effects on early initiation of natural convection in the vessel).
- Case 4: Reduction in the flow resistance in the core by a factor of 10 (to investigate increased air flow into the core).
- Case 5: No structural graphite oxidation in the lower reflector region (to maximized unreacted air in the active core region).
- Case 6: Thermal conductivity of the side reflector reduced by 50% (to investigate the effects of higher core temperature on core oxidation).
- Case 7: Infinite containment volume (to investigate ultimate unmitigated long term behavior).
- Case 8: A combination of all seven previous cases as the most conservative case.

## G.2 Introduction

A MELCOR model of a reference pebble-bed reactor (PBR) was developed to explore the environmental conditions for oxidation in the PBR core in the event that fuel elements and graphite core structural components are exposed to air due to a catastrophic break in the cross flow duct connecting the reactor pressure vessel (RPV) with the power conversion systems vessel. The break is assumed to occur outside of the reactor vessel between the RPV and the high-pressure turbine. The MELCOR model presented in this appendix is sufficiently representative of PBR designs to scope out environmental conditions in the core during an air ingress accident.

The MELCOR [G-2] code used for this analyses is a severe accident code being developed at Sandia National Laboratory for the U. S. Nuclear Regulatory Commission to model the progression of severe accidents in light-water nuclear power plants. The modeling approach used by MELCOR, like other thermo-hydraulic codes, is based on the use of control volumes, heat structures, control functions and material property tables to build system models. Because of the general and flexible nature of the code, other concepts such as the pebble-bed reactor can be modeled with some simple modifications to the code. The latest released version of MELCOR is 1.8.5; however, for the analysis presented in this report a modification of the earlier 1.8.2 version of the code was used. The modifications to MELCOR 1.8.2 were the implementation of multi-fluid capabilities, a graphite oxidation model, and a simple molecular diffusion model. The multi-fluid capabilities allow MELCOR to use fluids other than water, such as helium, as the primary coolant for low Mach number flows (gases that can be treated as an incompressible fluid). This capability is documented in Reference [G-3]. The capability to analyze the oxidation of graphite structures was also added to MELCOR and will be discussed later in this appendix as will the molecular diffusion model.

## G.3 PBR MELCOR Model

The PBR reactor considered for this study was assumed to have a core diameter of 3.5 m and a height of 8.0 m, yielding a total core volume of 76.97 $m^2$. The active core of the reactor was divided into three radial zones and eight axial zones for a total of 24 core control volumes, as shown in Figure G-1. The inner radial zone consists of 8 control volumes representing the inner reflector region (non heat generating). The remaining 16 core control volumes represent the active core. The core control volumes are cylindrical and are centered about the core centerline. The inner radial zone (inner reflector) contains 72,247 non-heated pebbles[1]. The two outer radial zones contain a total of 342,944 heat-generating pebbles producing a total of 270 MW of thermal energy. The pertinent dimensions for this model are given in Table G-1.

For nominal operating conditions the coolant enters the bottom of the reactor (CV111) at ≈ 450°C (723 K) and flows up an annular flow channel located between the reactor side reflector and the core barrel. Control volumes 101 through 110, and 211, 212, 213 as shown in Figure G-1 represent this flow channel. The coolant then flows radially along the top of the

[1] The most recent core design for the PBMR involves a fixed cylindrical graphite central column rather than moving solid graphite (unfueled) pebbles

reactor (CV 100), exiting into a small plenum located just above the core, represented by control volumes 25, 26, and 27.

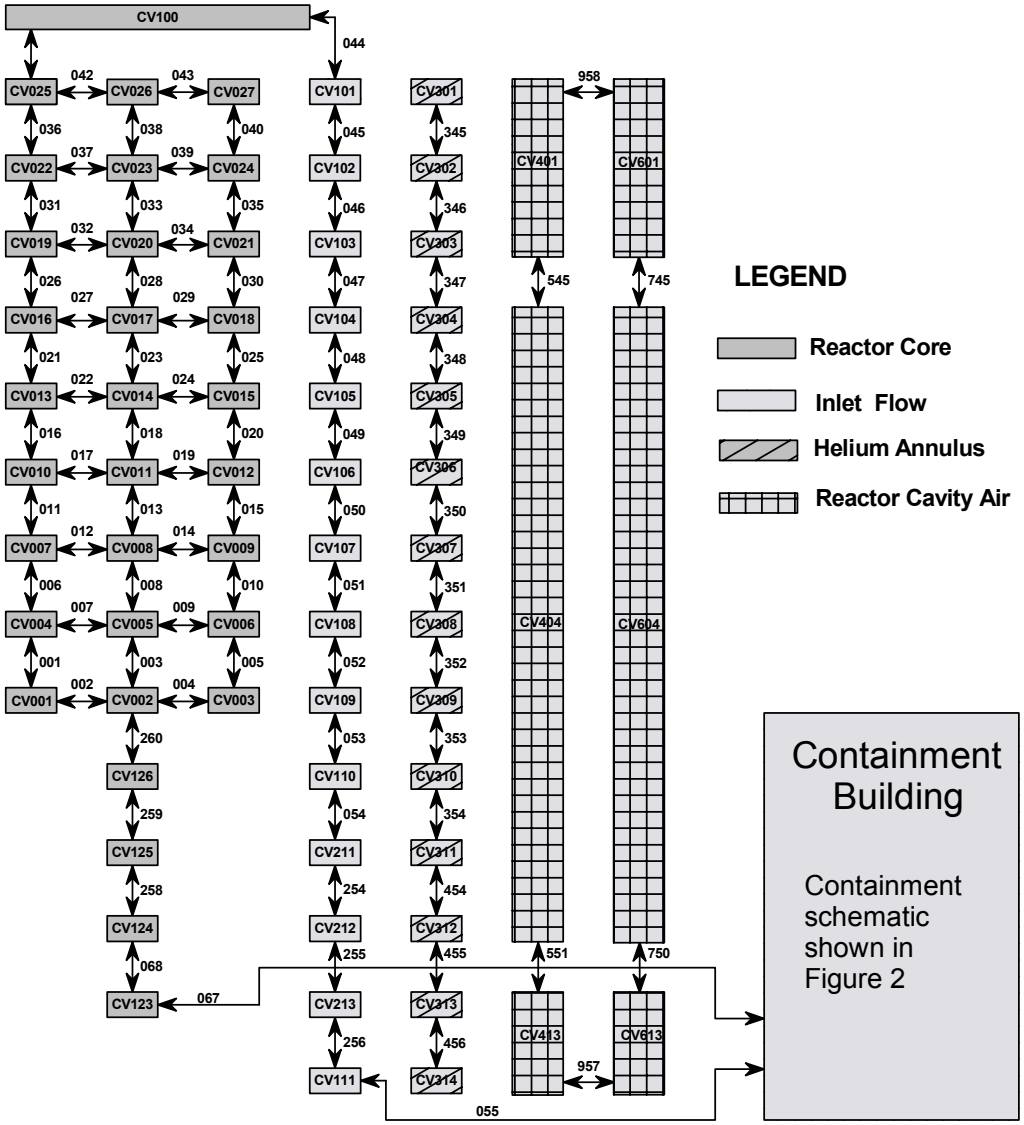


Figure G-1 PBR control volume diagram

From the plenum the coolant flows down through the core and exits the bottom of the core (CV126) at 850°C (1123 K). The coolant then flows down through the lower support structure (CVs 126, 125, 124, and 123) to the power conversion unit, which is represented simplistically by control volumes 112 through 122 (refer to Figure G-2). The double-ended rupture of both the inlet and outlet pipes as shown in Figure G-2 occurs in control volumes 112 and 122. The pipe break is represented in the model as two valves, which are connected to containment volumes 500 and 501 (not shown in figure) and are opened at the beginning of the loss of coolant accident (LOCA). This accident is sometimes referred to as a depressurized conduction cool down event.

For the base case model and all models used in the sensitivity study unless noted, the containment volume is assumed to be 27,000 $m^3$. This value was estimated from preliminary drawings of the containment region, thus the actual containment volume might be smaller. The large containment volume allows more oxygen to be available for oxidation of the core graphite.

**Table G-1 Summary of Basic Modeling Parameters for Air Ingress Sensitivity Study**

| Parameters | PBR Base Case | Units |
|---|---|---|
| Thermal Power | 270.0 | MW |
| Core coolant inlet temperature | 450.0 | °C |
| Core coolant outlet temperature | 850.0 | °C |
| Outer radius of inner flow zone [inner reflector] | 0.73 | m |
| Outer radius of middle flow zone | 1.21 | m |
| Outer radius of outer flow zone | 1.75 | m |
| Outer radius of radial reflector | 2.50 | m |
| Outer radius of inlet coolant channel | 2.80 | m |
| Outer radius of core barrel | 2.83 | m |
| Outer radius of gas annulus | 2.90 | m |
| Outer radius of pressure vessel | 3.00 | m |
| Inner radius of reactor cavity cooling system | 4.27 | m |
| Height of HS 124, 111, 714, 314, 414 | 1.20 | m |
| Height of HS 223, 210, 713, 313, 413 | 0.80 | m |
| Height of HS 224, 211, 712, 312, 412 | 0.50 | m |
| Height of HS 225, 212, 711, 311, 411 | 0.50 | m |
| Height of HS 226, 213, 710, 310, 410 | 0.50 | m |
| Height of CV 01, 02, 03 | 0.06 | m |
| Height of CV 04, 05, 06 | 0.06 | m |
| Height of CV 07, 08, 09 | 0.18 | m |
| Height of CV 10, 11, 12 | 0.18 | m |
| Height of CV 13, 14, 15 | 0.36 | m |
| Height of CV 16, 17, 18 | 2.39 | m |
| Height of CV 19, 20, 21 | 2.39 | m |
| Height of CV 22, 23, 24 | 2.39 | m |
| Height of CV 25, 26, 27 | 0.50 | m |
| Number of non-fuel pebbles in reactor (inner reflector) | 72247 | - |
| Number of fuel pebbles in reactor | 342944 | - |
| Active height of core | 8.00 | m |
| Total volume of core | 76.97 | $m^3$ |
| Active core volume | 63.57 | $m^3$ |
| Core mean power density | 5.51 | $MW/m^3$ |
| Core mass flow rate (steady state) | 131.00 | kg/sec |

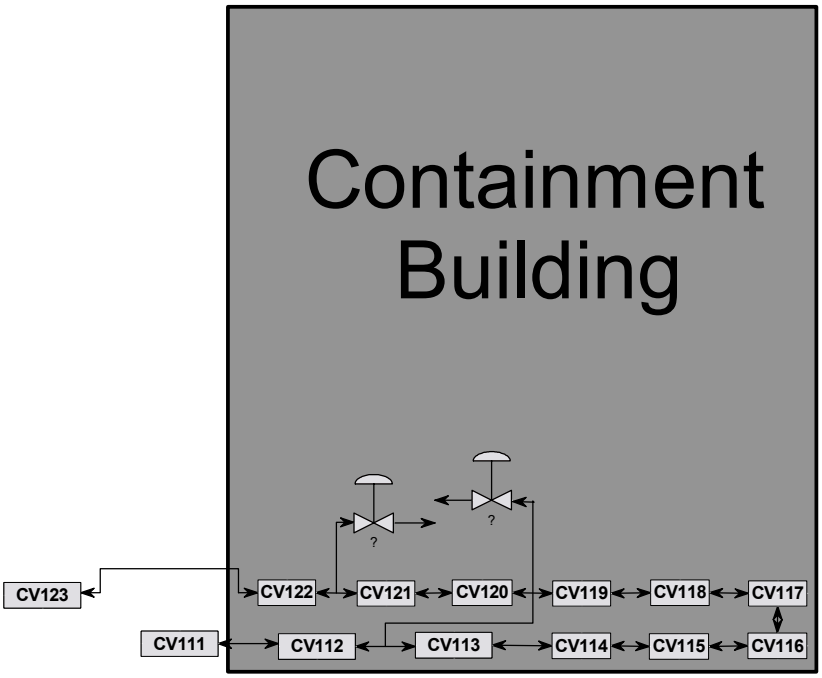


Figure G-2 PBR control volume diagram continued

The heat transfer from the pebbles is dominated by convection during normal operation. However, for the LOCA when the forced circulation flow in the core decreases to zero, the decay heat generated by the pebbles is removed primary by radial conduction and radiation to the graphite reflector, which surrounds the core. The heat is then conducted through the reflector, radiated and conducted to the primary reactor vessel (RPV) wall, conducted through the vessel wall, and is finally convected and radiated to the reactor cavity cooling system (RCCS), which for the purposes of this study was modeled as a 27°C (300 K) heat sink.

The reactor pebbles, and core structures such as the top, bottom, and side graphite reflectors, core barrel, reactor pressure vessel, and lower graphite support structures are modeled using the MELCOR heat structure package. The heat structure package calculates one-dimensional heat conduction through a solid structure and the energy transferred across its boundary surfaces into surrounding control volumes. Each heat structure has two boundary surfaces and a boundary condition must be specified for each surface. One of six different boundary condition can be specified depending on the modeling assumptions used at the boundary. For most of the surfaces in the model the heat transfer package calculates a convective heat transfer coefficient based on the flow conditions in the adjacent control volume and the geometry of the heat structure. Most of the heat structures used in the model are shown in Figure G-3 and are represented in the figure as rectangular boxes. An identifier beginning with the prefix HS denotes each heat structure. Each heat structure is coupled to at least one or two control volumes, which are identified on the figure as numbers in parentheses with the top number identifying the control volume located on the inside of the heat structure and the number on the bottom identifying the control volume on the outside of the heat structure. The wire like coupling between the heat structures represent radiation and conduction paths and are defined by control functions which will be discussed below.

The pebbles in the core are modeled as spherical heat structures, one heat structure per control volume. The convective heat transfer from one pebble is then multiplied by the number of pebbles in the control volume to get the overall convective heat transfer from all the pebbles in the volume to the fluid.

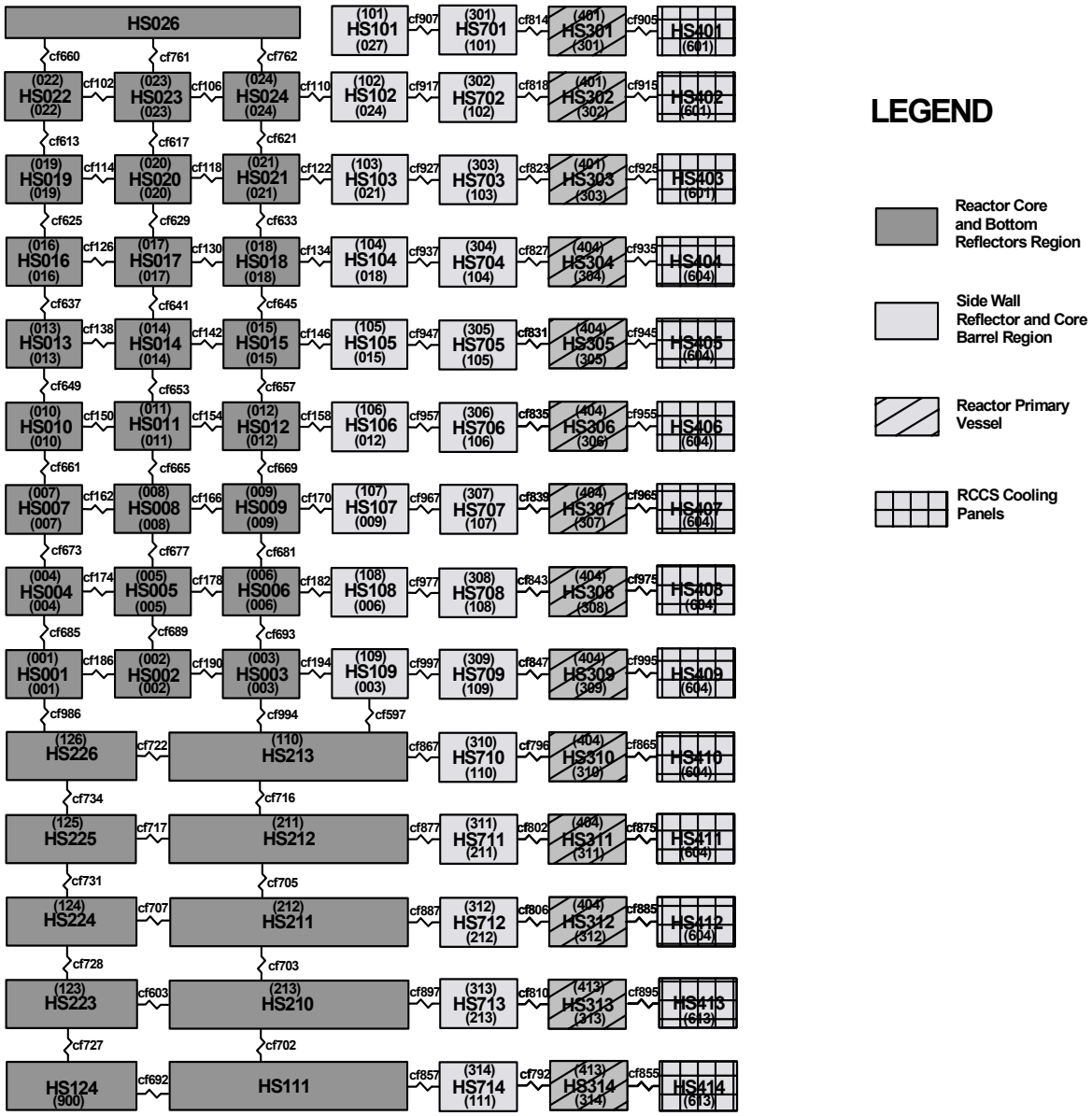


Figure G-3 PBR heat structure diagram

A control function in conjunction with a user-defined subroutine is used to model the axial and radial conduction and radiation heat transfer between the heat structures representing the pebbles in the core. The radial heat transfer rate between the heat structures in the core is governed by

$$\dot{Q}_{radial} = \frac{2\pi \cdot l \cdot k_{eff} \cdot \left(T_{r,z} - T_{r+1,z}\right)}{\ln\left(\frac{r_{r+1,z}}{r_{r,z}}\right)} \tag{1}$$

and the axial heat transfer rate between heat structures is governed by

$$\dot{Q}_{axial} = \frac{k_{eff} \cdot A_{cross}}{L}\left(T_{r,z} - T_{r,z+1}\right) \tag{2}$$

where $\dot{Q}_{radial}$ is the total radial heat transfer between CV(r,z) and CV(r+1,z), l is the height of the control volume, $r_{r+1,z}$ is the center radius of CV(r+1,z), $r_{r,z}$ is the center radius of CV(r,z), $k_{eff}$ is the effective thermal conductivity of the pebble bed, $\dot{Q}_{axial}$ is the the total axial heat transfer rate between CV(r,z) and CV(r,z+1), $A_{cross}$ is the cross sectional area between CV(r,z) and CV(r,z+1), and L is the length between the center of CV(r,z) and CV(r,z+1). The total radial heat transfer rate to CV(r+1,z) from CV(r,z) is divided by the number of pebbles in CV(r+1,z) to obtain the heat transfer rate per pebble entering CV(r+1,z). The total radial heat transfer rate from CV(r,z) to CV(r+1,z) is divided by the number of pebbles in CV(r,z) to obtain the heat transfer rate per pebble leaving CV(r,z). The same process is applied to the axial heat transfer rate. The heat source term is then added or subtracted to obtain the net heat conduction per pebble in appropriate control volumes per unit time. The effective thermal conductivity used in this study accounts for the radiation and conduction through the bed in both the axial and radial direction.

## G.4 Effective Thermal Conductivity

The active core of a pebble bed reactor is an annular packed bed of spherical fuel pebbles with each fuel pebble element containing many fuel particles. The heat from the pebbles is transported simultaneously by a combination of mechanisms. These mechanisms are radiation through the gas regions between the pebbles, conduction through the gas surrounding the pebbles, and the conduction through the pebbles. As described in Reference [G-4] the overall effective conductivity is calculated from three different individual effective conductivities. The individual effective conductivities are summed to obtain the overall effective conductivity of the core region. These three individual effective conductivities are defined as (1) void radiation plus solid conduction, (2) gas conduction plus solid conduction, and (3) contact conduction plus solid conduction.

Equation (3) describes the effective conductivity due to void radiation plus solid conduction and is based on the cell model defined by Zehner and Schlüender [G-5] and modified by G. Breitbach and Barthels [G-6].

$$\lambda_{er} = \left[ \left( 1 - \left(1-\varepsilon_p\right)^{\frac{1}{2}} \right) \cdot \varepsilon_p + \left( \frac{\left(1-\varepsilon_p\right)^{\frac{1}{2}}}{\frac{2}{\varepsilon_r} - 1} \right) \cdot \frac{B+1}{B} \cdot \frac{1}{1 + \frac{1}{\left(\frac{2}{\varepsilon_r} - 1\right) \cdot \Lambda}} \right] \cdot 4\sigma T^3 d \qquad (3)$$

where

$$B = 1.25 \left( \frac{1-\varepsilon_p}{\varepsilon_p} \right)^{\frac{10}{9}} \qquad (4)$$

$$\Lambda = \frac{\lambda_s}{4\sigma T^3 d} \qquad (5)$$

The variables in Eq.'s (3), (4) and (5) are $\sigma$ the Stefan-Bolzmann constant, $\lambda_s$ the thermal conductivity of the pebble matrix material, $\varepsilon_p$ the porosity of the pebble bed (0.39), $\varepsilon_r$ the emissivity of the pebble matrix material (0.8), d the diameter of the pebbles (6 cm), and T is the average temperature of the pebbles in the control volume.

The second term describes the effective conductivity due to gas conduction plus solid conduction. This equation was formulated by Zehner and Schlüender and tested by V. Prasad et, al [G-7].

$$\lambda_{eg} = \left[ 1 - \sqrt{1-\varepsilon_p} + \frac{2 \cdot \sqrt{1-\varepsilon_p}}{1-\lambda \cdot B} \cdot \left( \left( \frac{(1-\lambda) \cdot B}{(1-\lambda \cdot B)^2} \right) \cdot \ln\left( \frac{1}{\lambda \cdot B} \right) - \left( \frac{B+1}{2} \right) - \left( \frac{B-1}{1-\lambda \cdot B} \right) \right) \right] \cdot \lambda_g \qquad (6)$$

where

$$\lambda = \frac{\lambda_g}{\lambda_s} \qquad (7)$$

In equations (6) and (7) $\lambda_g$ is the thermal conductivity of gas in the space between the pebbles in the pebble bed.

The third term describes the effective conductivity due to contact conduction between pebbles plus solid conduction within the pebbles. The effective conductivity component is the result of compressive loads on the spheres due to the weight of the particles in the bed.

$$\lambda_{ec} = \left[ \frac{3 \cdot \left(1 - \mu_p^2\right)}{4 \cdot E_s} \cdot f \cdot \frac{d}{2} \right]^{\frac{1}{2}} \cdot \frac{1}{0.531 \cdot S_s} \cdot \left( \frac{N_A}{N_L} \right) \cdot \lambda_s \tag{8}$$

where

$$f = p \frac{S_F}{N_A} \tag{9}$$

For a bed assumed to have a simple cubic arrangement of the spheres, $S_S$, $S_F$, $N_A$ and $N_L$ are given as $S_S = 1$, $S_F=1$, $N_A = 1/(4R^2)$, $N_L=1/(2R)$ where R is the radius of a pebble. In Eq. (8) $\mu_p = 0.136$ and $E_S = 9.0E09$ ($N/m^2$). These two values are Poisson's ratio and Young modulus respectively. The variable p is the external pressure and is estimated by the weight of the pebbles in the pebble bed.

The effective thermal conductivity of the bed is the sum of the three terms given above:

$$k_{eff} = \lambda_{er} + \lambda_{eg} + \lambda_{ec} \tag{10}$$

The above equations were programmed into Mathcad [G-8] using temperature dependent helium[2] and graphite thermal conductivity to generate the effective thermal conductivity used in the pebble bed for this study. The effective thermal conductivity is shown in Figure G-4 and is labeled new effective conductivity in the figure. The effective conductivity model presented here has been validated by the SANA benchmark experiments (pebble bed experiments) performed in Germany and reported in Reference [G-4].

Also shown in the figure is a second curve (Old Effective Conductivity) corresponding to values calculated from a second correlation. The values corresponding to the second curve were used in one of the MELCOR calculations to obtain the sensitivity of the pebble bed oxidation to bed effective conductivity. The second effective thermal conductivity curve was calculated using the following equation, which is an old correlation, developed in the 1950s by General Electric as reported in Reference [G-9]. It was used in our original calculation presented in Reference [G-1].

$$k_{eff} = 1.1536 x 10^{-4} \left(T - T_o\right)^{1.6632} \tag{11}$$

where $k_{eff}$ has units of W/m-K and the temperature T has units of K. $T_o$ is a reference temperature equal to 273.16 K.

[2] The effect of air on the effective thermal conductivity of the core was not included in this study, however its effect would be to lower the effective thermal conductivity. The influence of air results should be bracketed by the two different effective thermal conductivity curves used in this study.

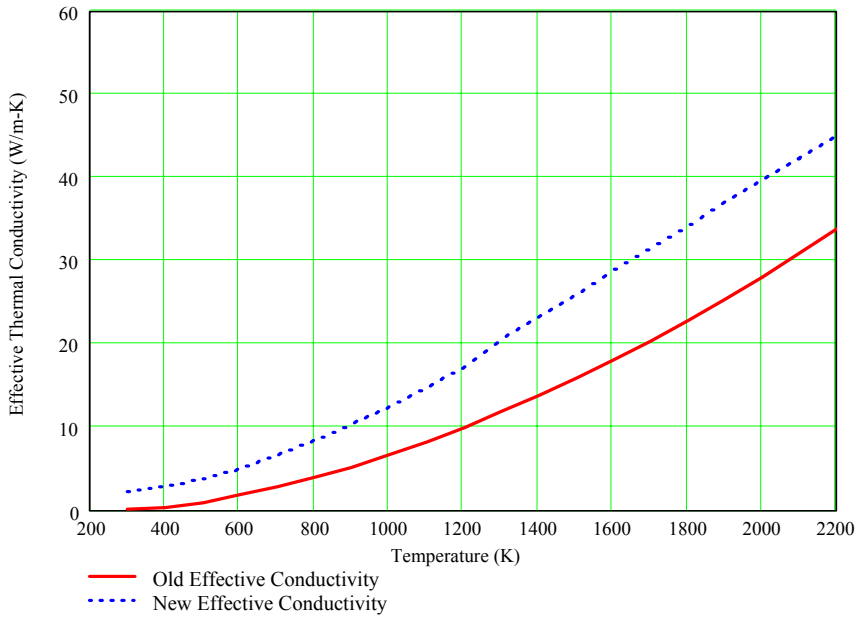


Figure G-4 Pebble bed effective thermal conductivity

The thermal conductivity of the fuel matrix used in equations (5), (7), and (8) was obtained from Reference [G-10] and is a function of both fast fluence, and the temperature at which the irradiation occurred. The fuel matrix thermal conductivity correlation presented in [G-10] was developed from experimental data from Germany and the United States. The equations presented in [G-10] were programmed into Mathcad and thermal conductivity curves (shown in Figure G-5) were generated. When compared to Figure 2.2 in Reference [G-10] the plots are identical.

Using a fast fluence of 1.5E21 neutrons/cm$^2$ for the core at an average core temperature of 923 K, the fuel matrix thermal conductivity curve shown in Figure G-6 was generated. The core fast fluence level was obtained from PEBBED, a neutronics code developed at the INEEL specifically for PBRs [G-11], [G-12]. The graphite conductivity for the side reflector was calculated (also shown in Figure G-6) using the same correlation for a 10-year fast fluence of 4.6E20 neutrons/cm$^2$ at an average temperature of 823 K. The side reflector fluence is lower than the fast fluence in the core region because of the very low fast flux in the reflector and was also obtained from the PEBBED code. The peak fast flux in the side reflector drops off rapidly with radius, thus a weighted average fluence value was calculated for use in calculating the outer reflector thermal conductivity. Shown in Table G-2 are fast flux values for five radial locations at the core midplane. The five fast flux values are area weighted and multiplied by 3.154E08 seconds to obtain a 10-year fluence value of 4.6E20 neutrons/cm$^2$

**Table G-2 Side Reflector Fast Flux Values**

| Radius (cm) | Fast flux (neutrons/cm$^2$*sec) | Cross sectional area (cm$^2$) | Columns 2*3 neutrons/sec |
|---|---|---|---|
| 182.5 | 6.09E12 | 1.720E04 | 1.047E17 |
| 197.5 | 1.63E12 | 1.861E04 | 3.034E16 |
| 212.5 | 4.39E11 | 2.003E04 | 8.792E15 |
| 227.5 | 1/17E11 | 2.144E04 | 2.509E15 |
| 242.5 | 2.65E10 | 2.286E04 | 6.057E14 |
| | | | |
| Total | | 1.001E05 | 1.470E17 |

$$\text{Fast Fluence} = \left(\frac{1.470\text{E}17}{1.001\text{E}05}\right) \cdot 3.154\text{E}08 = 4.6\text{E}20 \frac{\text{neutrons}}{\text{cm}^2}$$

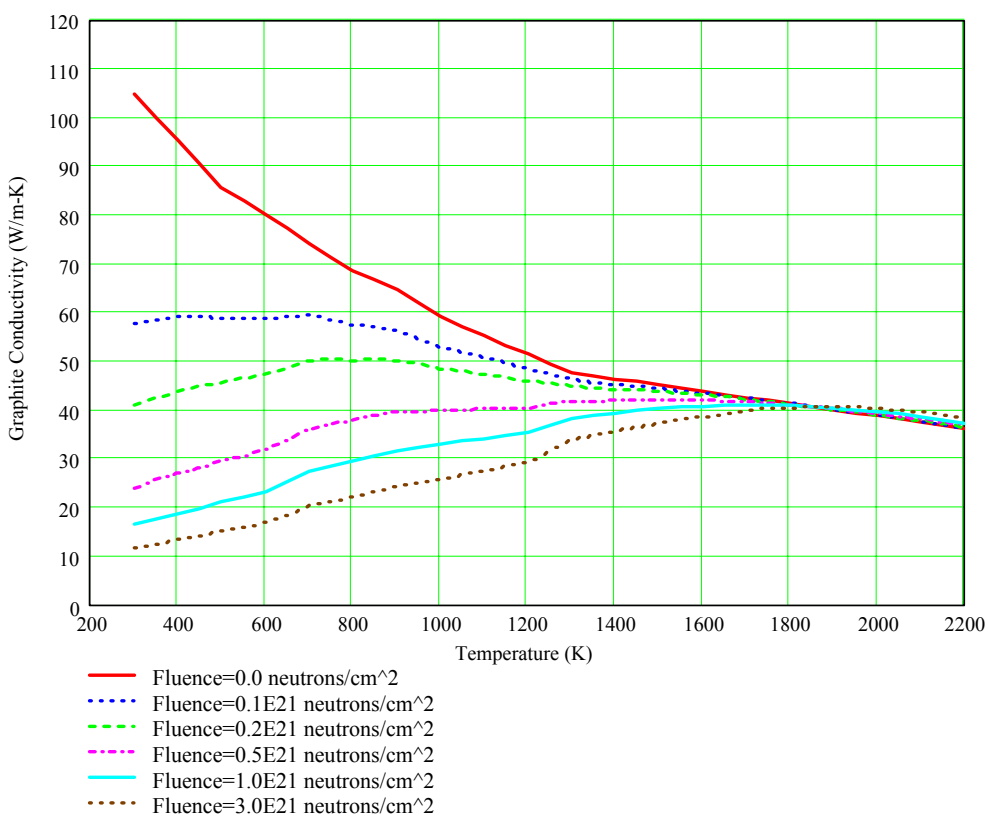


Figure G-5 Graphite thermal conductivity as a function of temperature and fast fluence

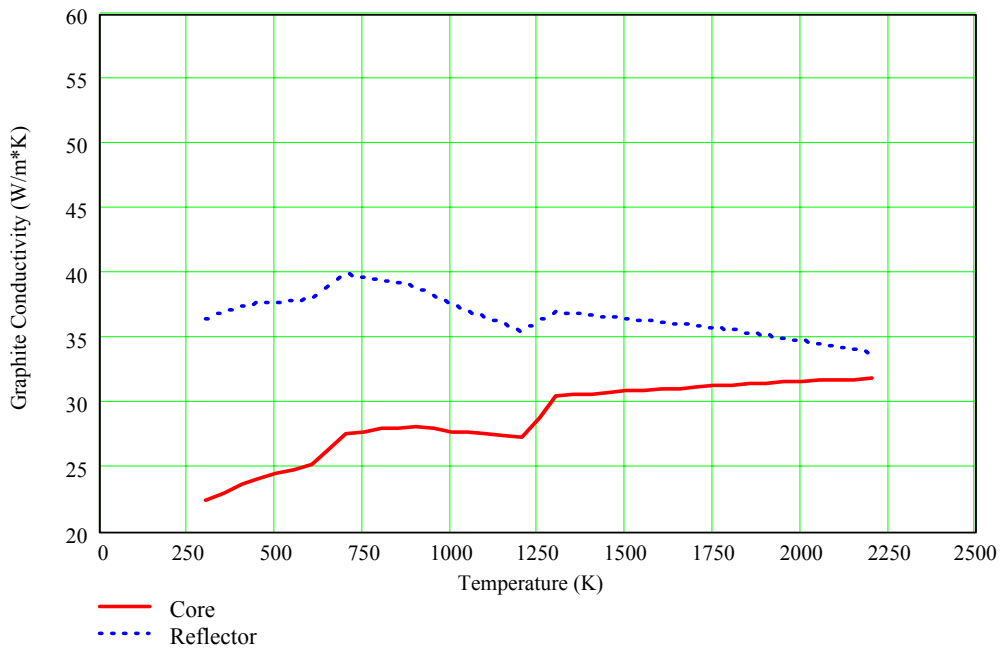


Figure G-6 Core and reflector graphite weighted average thermal conductivity verses temperature used in model

## G.5 Oxidation

Early experiments performed by Wicke [G-13] and Rossberg and Wicke [G-14] showed that the reactions between porous carbon and air could be divided into three reaction zones (regimes). The three zone are (1) the low temperature zone where the reaction is controlled by the reactivity of the carbon, (2) the intermediate temperature zone where the reaction is controlled by the diffusion of oxygen through the solid and (3) the high temperature zone where the reaction is controlled by the mass transport of the oxygen through the boundary layer surrounding the carbon specimen.

A subsidiary objective of this study was to understand the importance and sensitivity of graphite oxidation in the lower reflector and in attenuating the degree of oxidation in the other core regions caused by air ingress resulting from a LOCA. The oxidation model used for this study is based on the graphite oxidation rates data obtained experimentally at the INEEL [G-15, G-16]. The two-oxidation curves from References [G-15] and [G-16] are shown in Figure G-7, one corresponding to INEEL data generated in 1988 using a more porous graphite and the other to data generated in 2002 at the INEEL using a highly engineered carbon fiber composite (CFC). The reaction rates generated by the experiments in 2002 only covered the chemical kinetic control regime (Regime I) and the in-pore oxygen diffusion-controlled regime (Regime II). In order to cover all three regimes, the data from the 2002 experiment were combined with the data from the 1988 experiments. This resulted in a correlation that could be used over the entire temperature range and allowed a smooth transition between each regime. The resulting reaction rate curve for all three regimes, henceforth referred to as the INEEL-2002I curve, is presented in Figure G-7 and is the oxidation model used in this study. For the convenience of reading the

data the same data is plotted in Figure G-8 using a linear temperature scale for the x-axis as opposed to the inverse temperature scale used in Figure G-7.

For comparison purposes, some reaction rate data for German fuel pebble matrix material [G-17] are plotted in Figure G-8. The data are a function of the free stream velocity flowing past a pebble. Three curves are shown in Figure G-8 for free stream velocities of 0.043, 0.023 and 0.012 m/s. The German reaction rate data are higher in Regime I than the INEEL 2002 data. The reaction rates in Regime III are an order of magnitude lower than the INEL 1988 data. The German data are also limited to temperatures between 600 and 1200°C. Furthermore, the actual oxidation rate of graphite in the lower reflector is expected to be less than the German fueled pebbles shown here because the higher graphitization temperature of the reflector graphite should make the reflector graphite less reactive. Our earlier work using both the 1998 and 2002 INEEL reaction rate data showed that these differences in reaction rates were of less importance in the oxidation transient because the amount of the core involved in the oxidation is quite limited and the reaction at these temperatures becomes starved of air fairly quickly. The ability to get air into the core was critical. As seen from the data presented in Figure G-8 there is a large variation in the experimental data. The reaction rate for the specified fuel pebble matrix material and selected reflector graphite for a specific application would be needed to more accurately assess the behavior in an air ingress event. The INEEL 2002I oxidation curve was chosen for this study because the lower reaction rates in Regime I will allow more unreacted oxygen from the natural convecting airflow to reach the core. Most of the graphite temperatures in the lower reflector region are low enough that they fall within Regime I. Thus, the INEEL 2002I correlation was judged to be acceptable for these scoping studies.

The reaction rate equations programmed into MELCOR for the three regimes are:

Regime I: ($525 \le T < 710$ °C)

$$R_{ox} = 1.4754E07 \cdot \exp\left(-\frac{2.6128E04}{T}\right) \tag{12}$$

Regime II: ($710 \le T < 1175$ °C)

$$R_{ox} = 36.308 \cdot \exp\left(-\frac{1.3475E04}{T}\right) \tag{13}$$

Regime III: ($1175 \le T \le 1720$ °C)

$$R_{ox} = 1.57E-02 \cdot \exp\left(-\frac{2260.0}{T}\right) \tag{14}$$

The rate equations (12, 13, and 14) are based on the oxygen content in air at standard atmospheric conditions; thus, in the MELCOR model as a first-order approximation, the oxidation rates are assumed to vary linearly with the oxygen partial pressure as shown below:

$$R_{rate} = \frac{P_{ox}}{0.181E05\,Pa} R_{ox} \tag{15}$$

where $P_{ox}$ is the partial pressure of the oxygen in the flow and the constant 0.181E05 Pa is the atmospheric partial pressure of oxygen at the INEEL where the experiments were conducted.

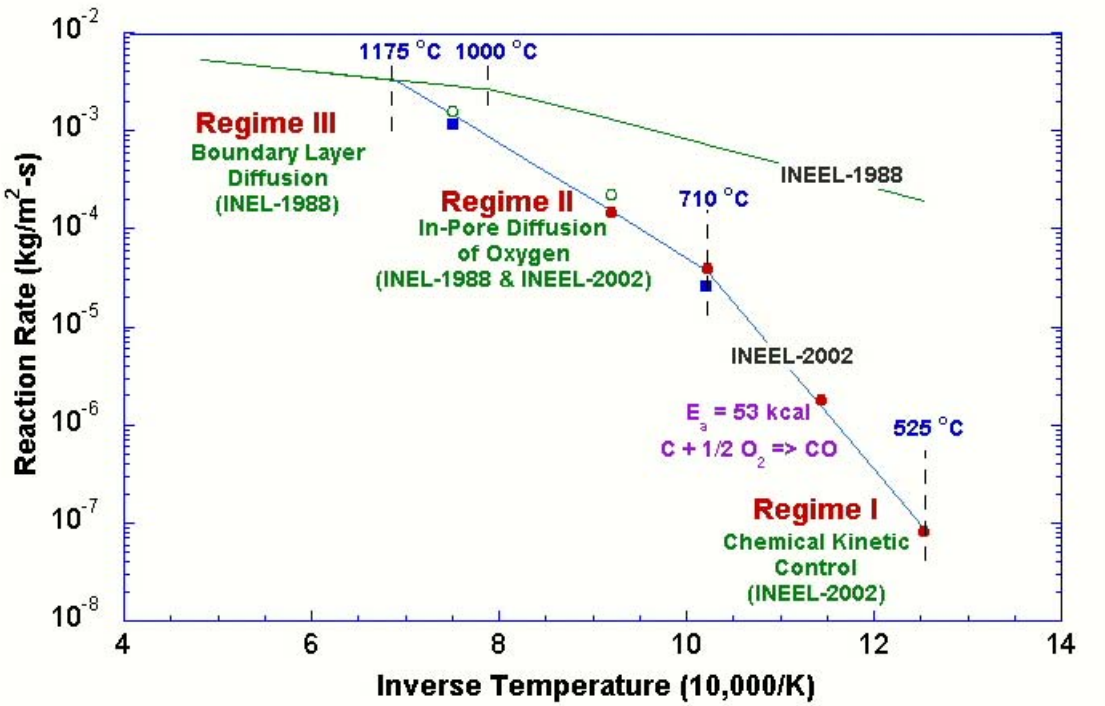


Figure G-7 CFC-air reaction rate curve for air ingress sensitivity studies.

The heat generated per pebble from the oxidation reaction is

$$q_{ox} = R_{rate} \cdot \Delta H_f \cdot A_{surface} \tag{16}$$

where $\Delta H_f$ is the heat of formation of carbon dioxide and $A_{surface}$ is the surface area of the pebble. The heat of formation of carbon dioxide is given as

$$\Delta H_f = 0.09516 \cdot \left( -93690. - 0.7077 \cdot T + 7.0E-07 \cdot T^2 - \frac{4.6E05}{T^2} \right) \text{ (kJ/kg)} \tag{17}$$

The temperature has the units of K.

During the oxidation of graphite, some CO will likely be generated but is not included in the graphite oxidation model that is presently in MELCOR. At these temperatures the CO may oxidize in the boundary layer. This assumption is conservative from the standpoint of maximum pebble temperatures since the heat of formation of $CO_2$ is greater than the heat of formation of CO.

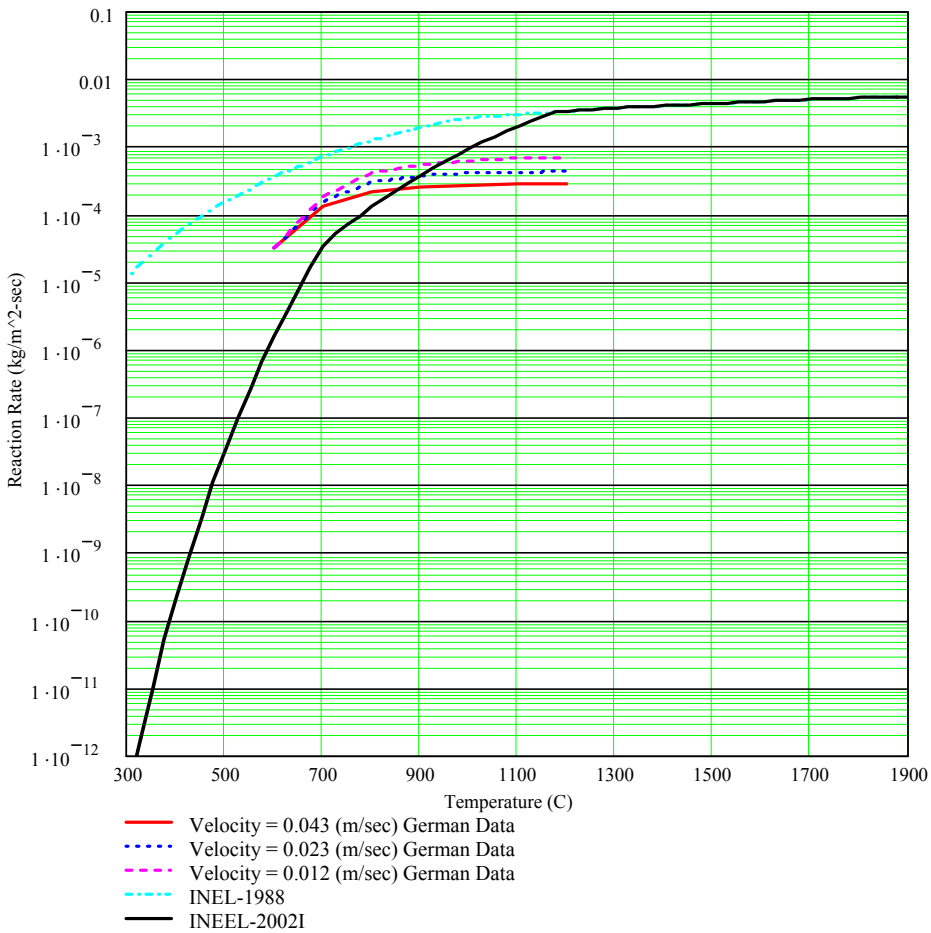


Figure G-8 Comparison of oxidation rate curves for INEEL-2002I, INEL-1988 and German pebble fuel element matrix data

## G.6 Diffusion Model

A diffusion model was added to the MELCOR code in order to simulate the molecular diffusion process, which occurs as air slowly diffuses into the helium present in the core prior to the onset of natural convection.

The differential equation expressing conservation of mass for the "ith" material solved by MELCOR [G-18] for the atmospheric phase of the fluid flow is:

$$\frac{\partial \rho_A^i}{\partial t} + \nabla \bullet (\rho_A^i \mathbf{v_A}) = \Gamma_A^i \qquad (18)$$

where

$\rho^i_A$ = atmosphere material density (kg/m$^3$)

$v_A$ = atmosphere flow velocity (m/s)
$\Gamma^i_A$ = atmosphere material source term[3] (kg/m$^3$-s)

Equation (18) was modified by adding a gaseous diffusion term that obeys Fick's Law of diffusion as follows:

$$\frac{\partial \rho^i_A}{\partial t} + \nabla \bullet (\rho^i_A \mathbf{v_A}) = \nabla \bullet \rho_A \, D^i_A \nabla \omega^i_A + \Gamma^i_A \qquad (19)$$

where

$D^i_A$ = mass diffusivity (m$^2$/s) for the "ith" material diffusing through the atmosphere phase (A) of the fluid flow
$\omega^i_A$ = mass fraction of the "ith" material = $\rho_i/\rho_A$

In MELCOR these equations are solved for control volumes (volumes defined by average material properties such as rooms) that are interconnected by flow paths (connections between volumes such as piping). After integrating Equation (19) over the "jth" control volume, the result is as follows:

$$\frac{\partial M^i_{j,A}}{\partial t} = \sum_k \sigma_{j,k} \, \alpha_{k,A} \, \rho^{i,d}_{k,A} \, v_{k,A} \, F_k \, A_k + \sum_k \rho_{k,A} \, D^i_{k,A} \left( \frac{\omega^i_{m,A} - \omega^i_{j,A}}{L_k} \right) \alpha_{k,A} F_k \, A_k + \dot{M}^i_{j,A} \quad (20)$$

Here, as described in Reference [G-18], M is the total mass; subscript k refers to a given flow path, with $\sigma_{j,k}$ accounting for the direction of flow in flow path k with respect to volume j; $\alpha_{k,A}$ is the volume fraction of the atmospheric phase in flow path k; superscript d denotes "donor", corresponding to the control volume from which the material is flowing; A is the flow path area; F is the fraction that the flow area is open; $L_k$ is the length of flow path k, and $\dot{M}$ includes all sources of mass. The diffusion coefficients for Equation 20 are calculated by MELCOR as described in Reference [G-19].

The diffusive term of Equation (20) is evaluated explicitly in time prior to each time advancement by MELCOR, and added to the mass source term as follows:

$$\dot{M}^{i \quad t_o+\Delta t}_{j,A} = \sum_k \rho_{k,A} \, D^i_{k,A} \left( \frac{\omega^i_{m,A} - \omega^i_{j,A}}{L_k} \right) \alpha_{k,A} F_k \, A_k + \dot{M}^{i \quad t_o}_{j,A} \qquad (21)$$

where $t_o$ is the time (s) at the start of a given computational time interval, and $\Delta t$ is the size of the next computational time interval (s) MELCOR has decided to take. Because an explicit update of the diffusive term has an upper stability limit regarding time interval size, defined per flow path as $L_k^2/D^i_{k,A}$, the maximum allowed time interval is determined for all flow paths and if the MELCOR adopted time interval exceeds this diffusive limit then the calculation is terminated

[3] Includes changes resulting from chemical reactions

with an error message stating that the maximum diffusive time step size has been exceeded. The remaining terms of Equation (20) are advanced in time as described in Reference [G-18].

## G.7 Core Pressure Drop

A significant determinant of the mass flow rate of air (oxygen) through the core following the onset of natural convection flow is the pressure drop through the core. The friction pressure drop $\Delta P_f$ through a pebble bed of height H can be expressed as

$$\Delta P_f = \psi \cdot \frac{H}{d_h} \cdot \frac{\rho_{ave}}{2} \cdot U_p^2 \tag{22}$$

where $\psi$ is the pressure drop coefficient, H is the height of the core, $d_h$ is the hydraulic diameter, $\rho_{ave}$ is the average density of the fluid in the core, and $U_p$ is the mean velocity in the gaps between the particles. The pressure drop coefficient is a function of the Reynolds number, which is defined as

$$Re_h = \frac{d_h \cdot U_p \cdot \rho_{ave}}{\mu} \tag{23}$$

where $\mu$ is the dynamic viscosity of the fluid.

The dependency of $\psi$ on the Reynolds number is

$$\psi = \frac{320}{\frac{Re}{1-\varepsilon}} + \frac{6}{\left(\frac{Re}{1-\varepsilon}\right)^{0.1}} \tag{24}$$

where

$$Re = \frac{d \cdot U \cdot \rho_{ave}}{\mu} = (1-\varepsilon) \cdot Re_h \tag{25}$$

In version 1.8.2, MELCOR calculates the frictional pressure drop through the core as

$$\Delta P_f = \frac{1}{2} \cdot \rho_{ave} \cdot U^2 \cdot \left(\frac{4 \cdot f \cdot H}{D}\right) \tag{26}$$

where f is the Fanning friction factor. In the MELCOR model, the pebble bed friction pressure drop (Equation 22) was approximated by a defined laminar flow coefficient for the specific flow

path. For laminar flow in a pipe, the value of the laminar flow coefficient is 16 and the Fanning friction factor equals this flow coefficient divided by the Reynolds number (e.g., f = 16/Re). For this study the Fanning laminar flow coefficient for the pebble bed region of the model was set at 175, which results in a pressure drop through the core of ≈ 46 Pa (shown in Figure G-9) for a mass flow of 0.125 kg/sec. This value of the laminar flow coefficient was found by programming Equations (22), (23), (24), and (25) into Mathcad and employing an iterative procedure to converge the flow coefficient to give the correct pressure drop at a specified mass flow rate. For a mass flow of 0.125 kg/sec the Mathcad model calculated the pressure drop as 43.2 Pa, which is in good agreement with the pressure drop calculated by MELCOR. This mass flow rate is approximately three times larger than calculations presented in Reference [G-17], which shows mass flow rates of 0.04 kg/sec for similar diameter breaks. However, for this scoping study, the larger mass flow rates are considered adequate for the oxidation and the maximum temperatures in the core for what are considered reasonably conservative assumptions.

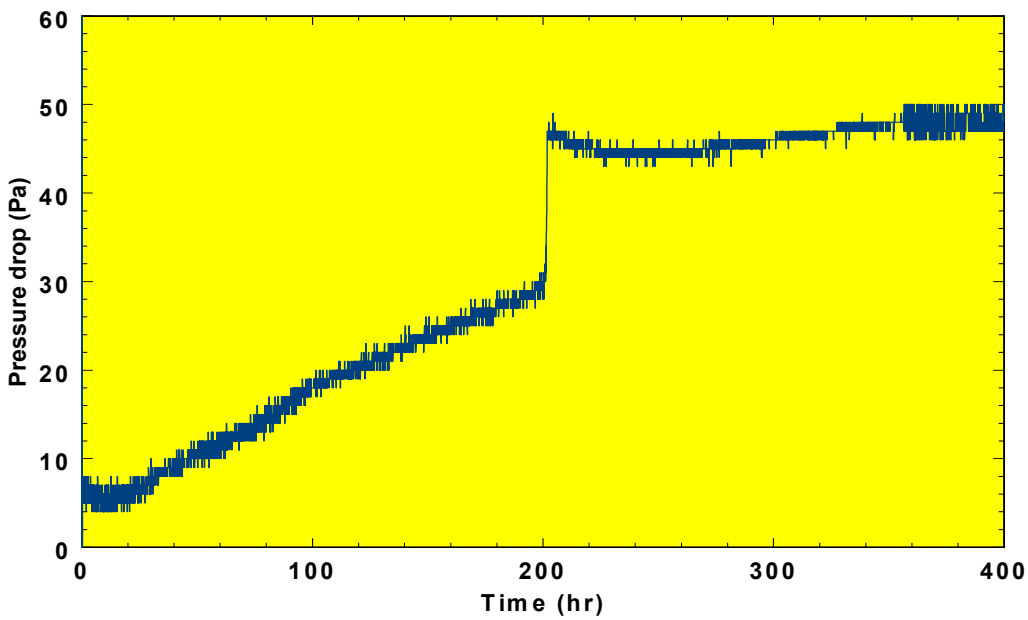


Figure G-9 Calculated core pressure drop following a large break LOCA

Equations (22), (23), (24), and (25) were programmed into Mathcad and for a mass flow of 0.125 kg/s, the pressure drop calculated was 43.2 Pa which is in good agreement with the pressure drop calculated by MELCOR.

## G.8 Results

The results for a base case analysis and seven sensitivity analyses where some factors were varied about their nominal values will be presented in this section. The base case model was constructed using nominal values for the reactor input variables such as the effective thermal conductivity in the core, the thermal conductivity of the graphite reflector sounding the core, the size of the containment containing the power conditioning equipment, and the flow resistance in

the core. A listing of the parameters that were varied is contained in Table G-3 as well as some of the results from the study. For the convenience of presenting the results the sensitivity calculations will be referred to as Case 1, Case 2 through Case 8. The cases are identified in Table G-3.

**Table G-3 Time and maximum temperatures by sensitivity analyses factor**

| Case | Sensitivity analyses factors | Lower region of lower reflector | Upper region of lower reflector | First (bottom) layer of pebbles | | | Upper active core region | | |
|---|---|---|---|---|---|---|---|---|---|
| | | Max Temp °C | Max Temp °C | Max Temp °C | Time Max Temp Occurred (hr) | Time above 1600 °C (hr) | Max Temp °C | Time Max Temp Occurred (hr) | Time above 1600 °C (hr) |
| 1 | Nominal value | 840 | 862 | 1611 | 209 | 0.3 | 1402 | 46 | 0 |
| 2 | Thermal conductivity in core varied | 840 | 852 | 1742 | 183 | 4.4 | 1499 | 52 | 0 |
| 3 | Small leak in upper head | 840 | 1087 | 1464 | 26 | 0.0 | 1388 | 42 | 0 |
| 4 | Core flow resistance reduced | 840 | 862 | 1745 | 228 | 3.1 | 1404 | 41 | 0 |
| 5 | No oxidation in lower reflector | 840 | 862 | 1611 | 209 | 0.3 | 1404 | 46 | 0 |
| 6 | Thermal conductivity in side reflector reduced by 50% | 848 | 867 | 1630 | 196 | 0.8 | 1529 | 61 | 0 |
| 7 | Infinite containment volume | 840 | 1317 | 1754 | 153 | 4.2 | 1407 | 46 | 0 |
| 8 | Factors all combined | 840 | 1091 | 1986 | 33 | 19.5 | 1618 | 64 | 46 |

The results from the base case analysis are presented in detail. The results from the other cases are presented in relation to their variation from the base case results.

### G.8.1 Case 1 – Base Case

The accident, which results in air ingress into the core and thus oxidation of the hot fuel pebbles, is a hypothetical loss of coolant accident (LOCA). The LOCA simulation was initiated at 1000 seconds by opening two valves in the MELCOR model (used to simulate the break in the pipes) that connect the hot and cold legs to the containment. The circulator tripped at 1000 seconds and the reactor was scrammed at the same time. The simultaneous double-ended rupture of the hot and cold legs causes a rapid depressurization of the primary coolant system. The pressure in the reactor equalizes with the containment pressure (0.15 MPa) in less than 3 seconds.

The mass flow rate of air through the core is shown in Figure G-10. After the depressurization stage, hot helium occupies the core, the upper and lower plenums, and the inlet coolant annulus of the reactor with cool heavy air at the entrance of the pipe breaks. In this configuration there is insufficient buoyancy force to support natural convective flow. Thus, little or no mass flow of air from the power conversion system building to the core and from the core to the power conversion system building occurs for a number of hours. During this phase of the accident, air from the power conversion system building is mainly transported to the reactor by molecular diffusion. Japanese and German experimental results support this delay or "incubation time" prior to the onset of natural convection [G-20, G-21].

The mass flow rate of air through the core is essentially zero until approximately 200 hrs. At this time, the mass fraction of air (nitrogen) has equalized between the core and the containment building causing the flow to suddenly increase from zero to 0.125 kg/s indicating the onset of natural circulation through the core. The flow rate through the core remains between 0.125 kg/s and 0.075 kg/s from 200 to 400 hours, the time when the transient was terminated.

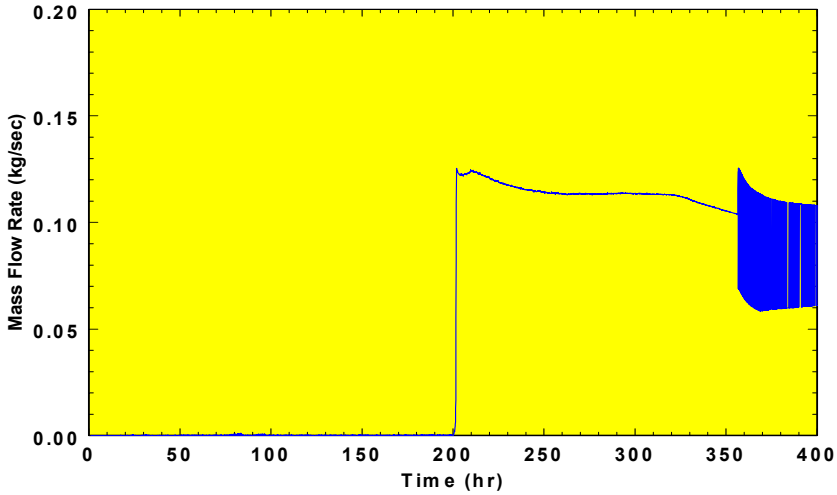


Figure G-10 Mass flow in the core after initiation of LOCA base case

The mole fraction of air (nitrogen) in the core and upper plenum of the reactor calculated by MELCOR gradually increases (shown in Figure G-11) until the buoyancy force is large enough to initiate natural circulation. The flow of air is from the hot leg to the cold leg upward through the core. As depicted in the figure, the mole fraction of nitrogen in the core gradually increases

from zero at the beginning of the accident to ≈ 0.45 by means of molecular diffusion. At this point natural convection starts and the mole fraction of nitrogen increases rapidly to 0.62, which is the value of the mole fraction of nitrogen in the containment after blow down. When natural convection starts, the mole fraction of oxygen in the containment immediately starts to decrease with a corresponding increase of carbon dioxide in the containment. This increase in carbon dioxide indicates that oxidation of the graphite in the reactor is occurring. The decrease in oxygen in the containment results from the assumption that there is no significant in leakage or out leakage of air in the containment building (i.e. the containment is assumed to reclose or be reclosed within a few days after the LOCA).

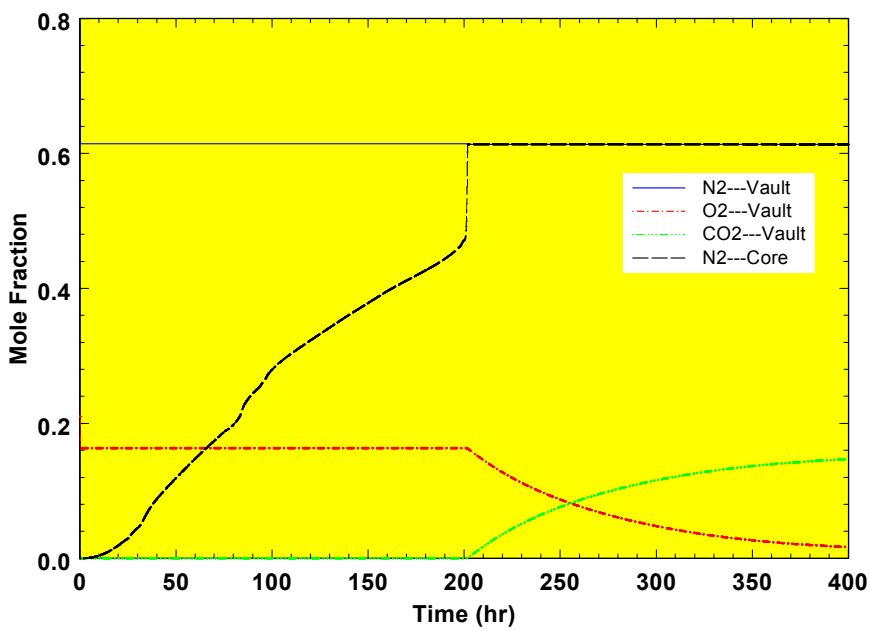


Figure G-11 Mole fraction of gas components in the reactor and containment

Figure G-12 is a schematic of the core and lower reflector region with arrows providing a correspondence between the temperature calculated by MELCOR and the physical location in the reactor. The temperature curves in all the figures to be discussed pertain to this schematic. When natural circulation of the air through the core begins, the temperature of the upper region of the lower reflector graphite (located below the active fueled core) immediately experiences a sharp rise in surface temperature as shown in Figure G-12. This rise in temperature is due mainly to conduction and radiation from the pebbles located at the entrance to the core as is discussed later when the results from the case of no oxidation in the lower reflector region is presented. As shown in Figure G-12, the temperature of the graphite reflector surface increases, from 490 $^{o}$C to a maximum of

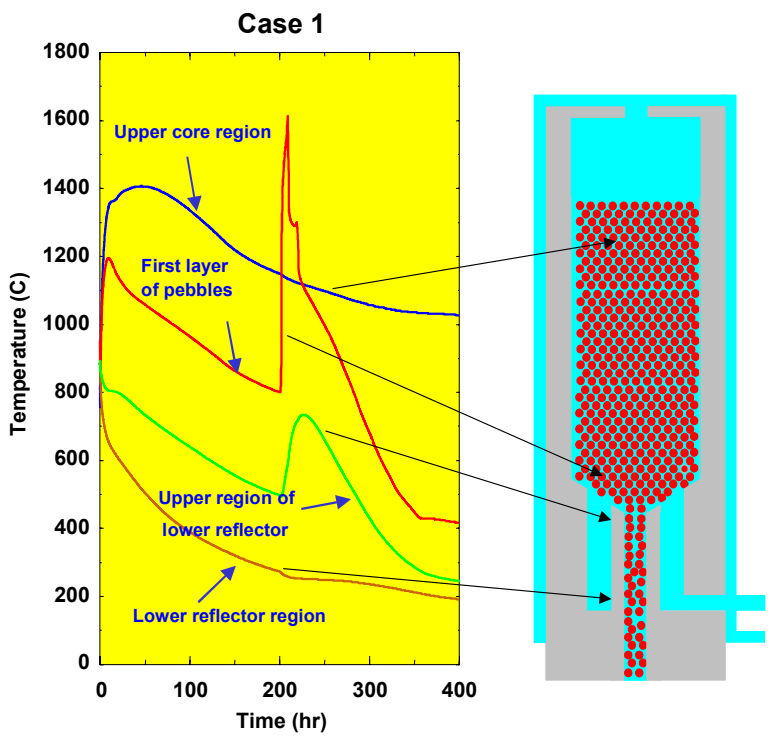


Figure G-12 Temperature history of the core and lower reflector region (base case)

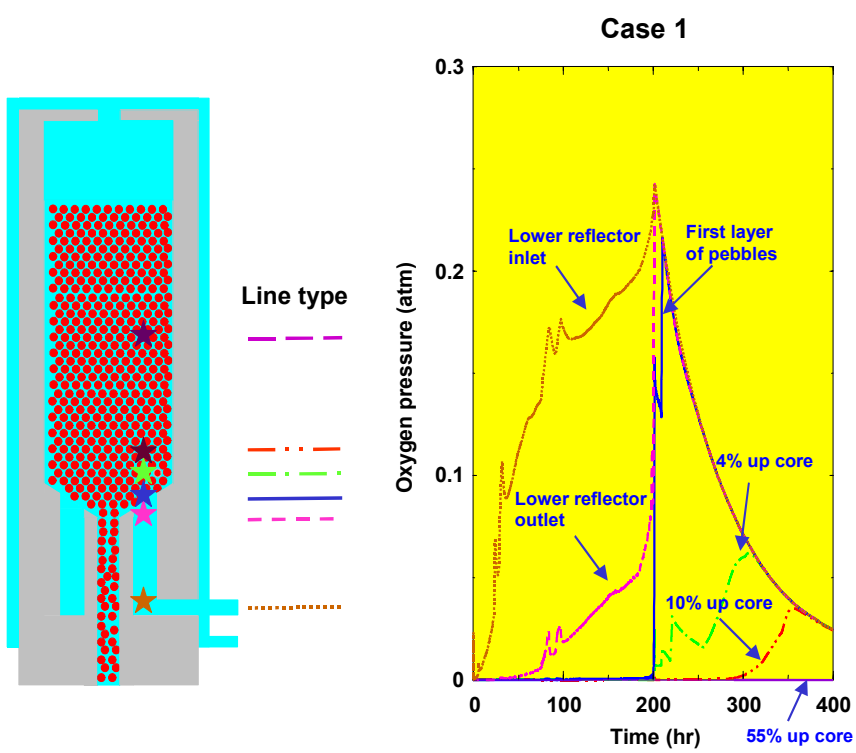


Figure G-13 Oxygen partial pressure history of the core and lower reflector region (base case)

733°C in 26 hours. At 226 hours the upper region of lower reflector graphite starts to cool down because the temperature of the pebbles in lower region of the core start to cool down. The graphite in the lower region of the lower reflector experiences initial no oxidation because the surface temperature of the graphite at the time of air ingress is 267 °C. This is substantially below the temperature at which significant oxidation takes place. This is consistent with the low oxidation rates (below $10^{-12}$ kg/m$^2$-sec) presented in Figure G-8 for temperature below 300 °C.

During the first 200 hrs of the event, the bottom layer of pebbles in the reactor core initially increases significantly and reaches a temperature of 1200°C at 9 hours and then begins to cool down reaching a temperature of 500°C at 200 hours. At 200 hours, natural convection starts and the surface temperature of the pebbles in the bottom layer rapidly increases as a result of oxidation of the graphite. The temperature increases from 500°C at 200 hrs to 1611°C by 209 hours. The temperature then begins to decrease again because the oxygen in the containment is depleted, i.e., the partial pressure of the oxygen in the first layer region has started to decrease as seen in Figure G-13. The pebble temperatures in CV(002) of the first layer are only above 1611°C for approximately 0.3 hours. The heated pebbles in the radially adjacent control volume (CV(003)) remain below 1600°C. As seen in Figure G-12 the pebbles in the upper core region experience no oxidation as indicated by no perturbation in the surface temperature plot. The maximum temperature that the pebbles in the upper region of the core experience during the transient is 1400°C. This temperature occurs at 45 hours and is due entirely to decay heating. In the base case only the control volume associated with the bottom layer of pebbles experience temperatures (slightly) in excess of 1600°C[4]. This control volume corresponds to 0.3% of the total fuel pebbles in the core.

Figure G-13 is a schematic of the lower reflector and core region. The stars (*) indicate the locations in the reactor where the partial pressure curves apply. The partial pressure curves in all the figures for all the cases to be discussed can be referenced to the star location in this schematic. Also shown in Figure G-13 is a plot of oxygen partial pressures at various locations in the lower reflector region and the core for the base case. The oxygen partial pressure curves are for the lower reflector inlet, the lower reflector outlet, the first layer of pebbles, 4% of the way up the core (Top of CV(008)), 10% of the way up the core (Top of CV(014)), 55% of the way up the core (Middle of CV(020)). The partial pressure at the lower reflector inlet slowly increases from 0.0 to 0.24 atm due mainly to molecular diffusion over the 200-hour period when there is no airflow to the core. An oxygen partial pressure of 0.24 atm is the value of the partial pressure in the containment before natural convection begins. As indicated in Figure G-13 there is little oxidation occurring in the lower region of the lower reflector. Thus, the decrease of oxygen partial pressure in this region is due to the corresponding decrease of oxygen partial pressure in the containment.

The oxygen partial pressure in the upper region of the lower reflector increases slowly due to molecular diffusion at a rate controlled by the concentration of oxygen in the lower region of the lower reflector. Although oxygen is available, the concentration (partial pressure) and the temperature of the graphite are low enough that no noticeable oxidation occurs prior to the onset of natural convection. When natural convection occurs the partial pressure of the oxygen

[4] In all cases time above 1600°C is presented as an indicator of the potential degradation of fuel

increase immediately to 0.24 atm, then follows the same partial pressure curve as the containment. Viewing Figure G-13 we see that very little oxygen is transported above 4% of the core (CV(008)). Thus, for the base case most of the oxygen is consumed in the bottom 4% of the core.

### G.8.2 Case 2 - Reduced Core Effective Thermal Conductivity

The sensitivity analysis corresponding to Case 2 consisted of using a different correlation for the effective core thermal conductivity resulting in a drop in the thermal conductivity of the pebble bed (see Figure G-4) that is approximately 30 to 35% lower in the temperature range of 1200 K to 1800 K than that used in the base case analysis. The temperature and oxygen partial pressure results for Case 2 are shown in Figures 14 and 15. Each figure has Case 1 results included for ease of comparison. The reduced core effective thermal conductivity results in approximately a 100 K increase in the core maximum temperatures. The flow of air from the containment to the core starts at 175 hours as opposed to 200 hours for the base case. As a result of the earlier occurrence of air flow to the core and the higher core temperatures, the temperature of the bottom layer of pebbles peaks at 1742°C and remains above 1600°C for 4.4 hours. The maximum temperature in the upper core peaks at 1500°C due to decay heating with no indication of any oxidation occurring in the upper regions of the core.

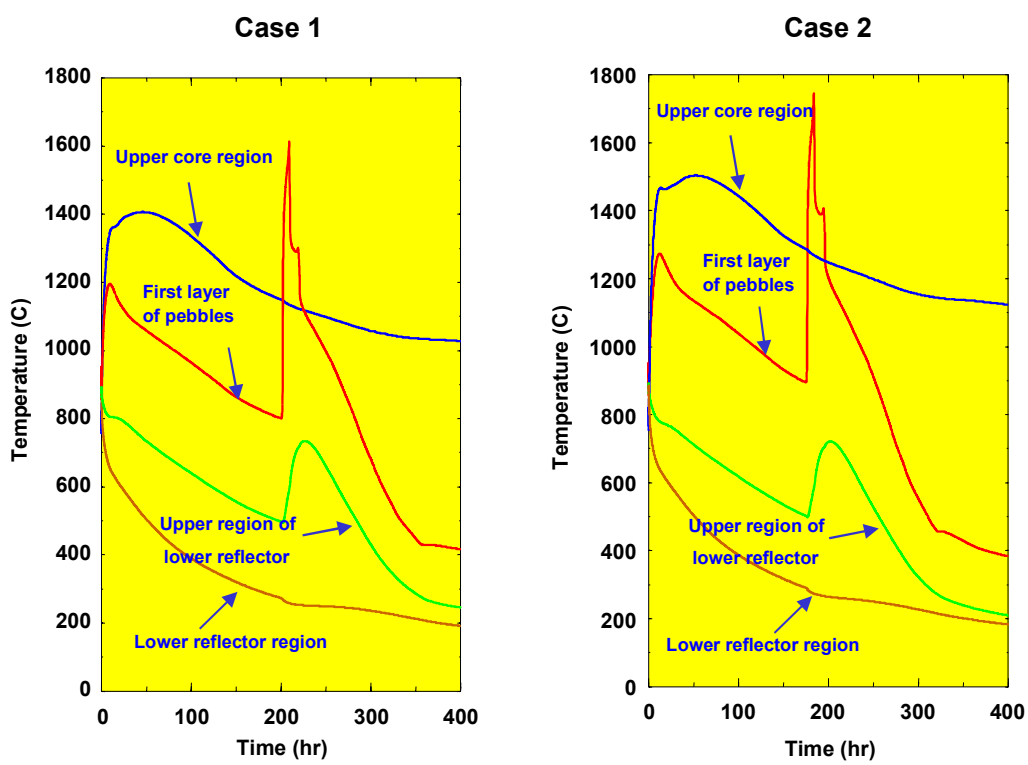


Figure G-14 Temperature history of the core and lower reflector region (Case 2)

Viewing Figure G-15, there is very little difference in the general shape of the oxygen partial pressure curves between Case 2 and the base case. The partial pressure of oxygen 4% of the way up the core is 0.057 atm for Case 2 and is 0.060 atm for Case 1. Due to the higher temperature in

the first several layers of pebbles more oxygen is consumed in the lower regions of the core for Case 2 than in the base case. Only approximately 0.3% of the core experiences temperatures in excess of 1600°C.

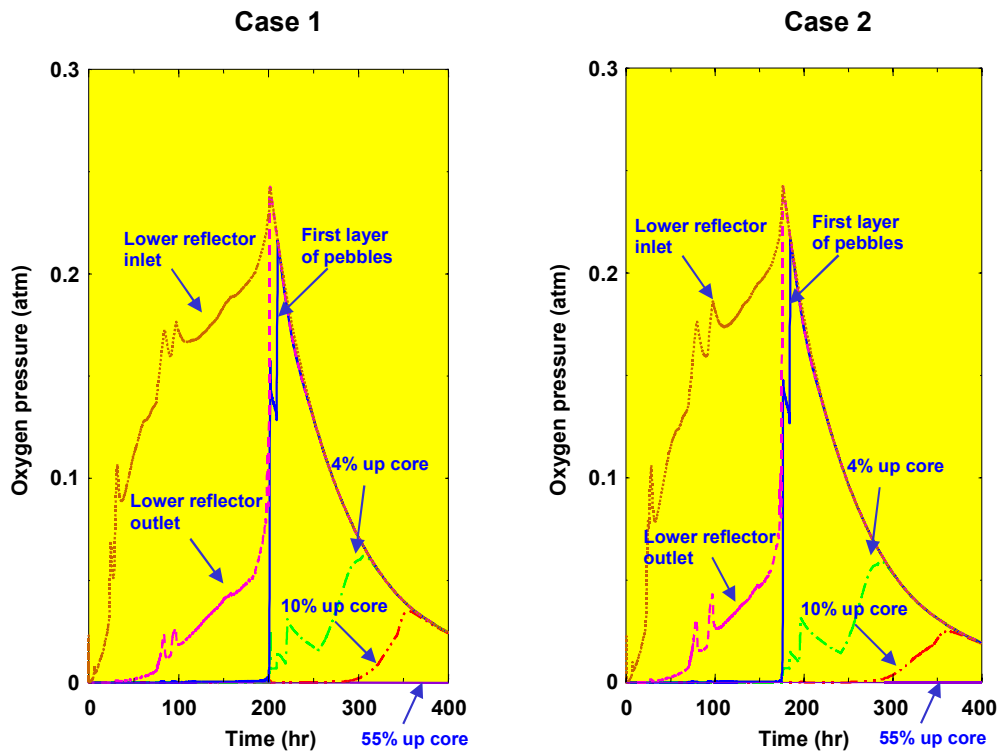


Figure G-15 Oxygen partial pressure history of the core and lower reflector region (Case 2)

### G.8.3 Case 3 - Significant Leak in the Reactor Vessel Upper Head

Case 3 assumes a significant leakage in the upper head of the reactor at the time of the LOCA. The leak results in a 15% per day loss of helium mass from the reactor to the air between the RPV and containment building for a maximum pressure differential of 6.9 MPa. This leak causes the onset of natural convection to occur much earlier (22 hours) in the event when compared to the base case (200 hours). The temperature and oxygen partial pressure results corresponding to Case 3 are presented in Figures 16 and 17 respectively. The temperatures in the lower region of the lower reflector are approximately the same as in the base case because the temperatures are too low for any oxidation to occur. The time-temperature history of the bottom layer of pebbles is substantially different between Case 3 and Case 1. The temperature of the bottom layer of pebbles immediately starts to increase as the flow of oxygen from the containment reaches the bottom of the core. However the temperature of the pebbles in the bottom

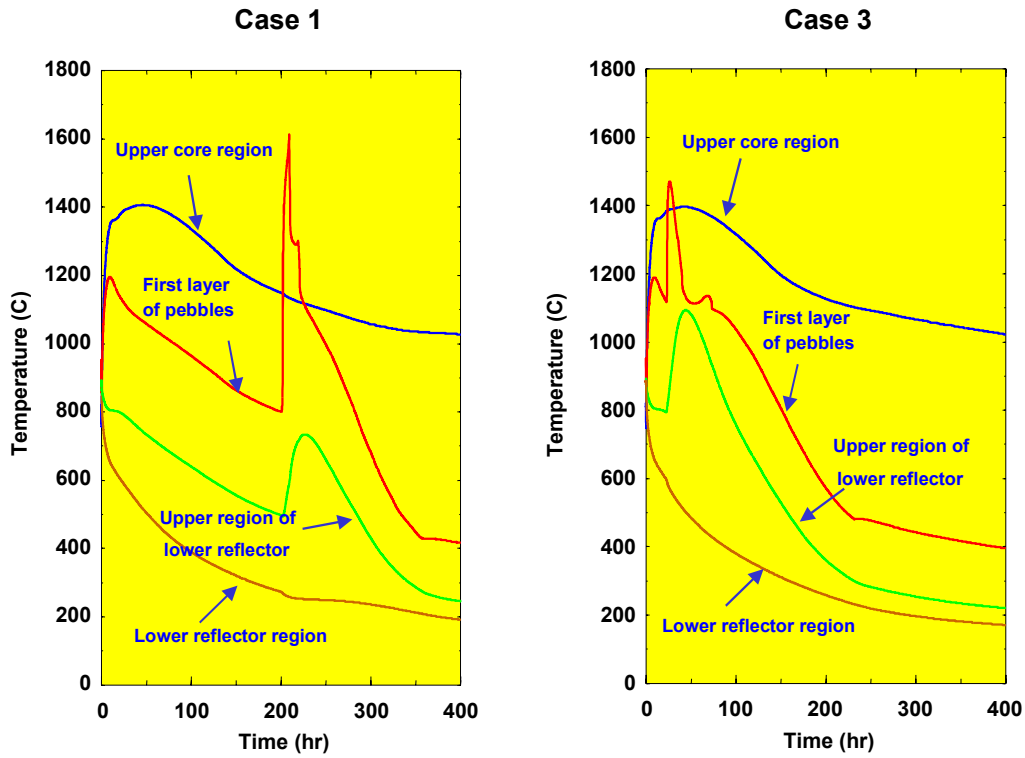


Figure G-16 Temperature history of the core and lower reflector region (Case 3)

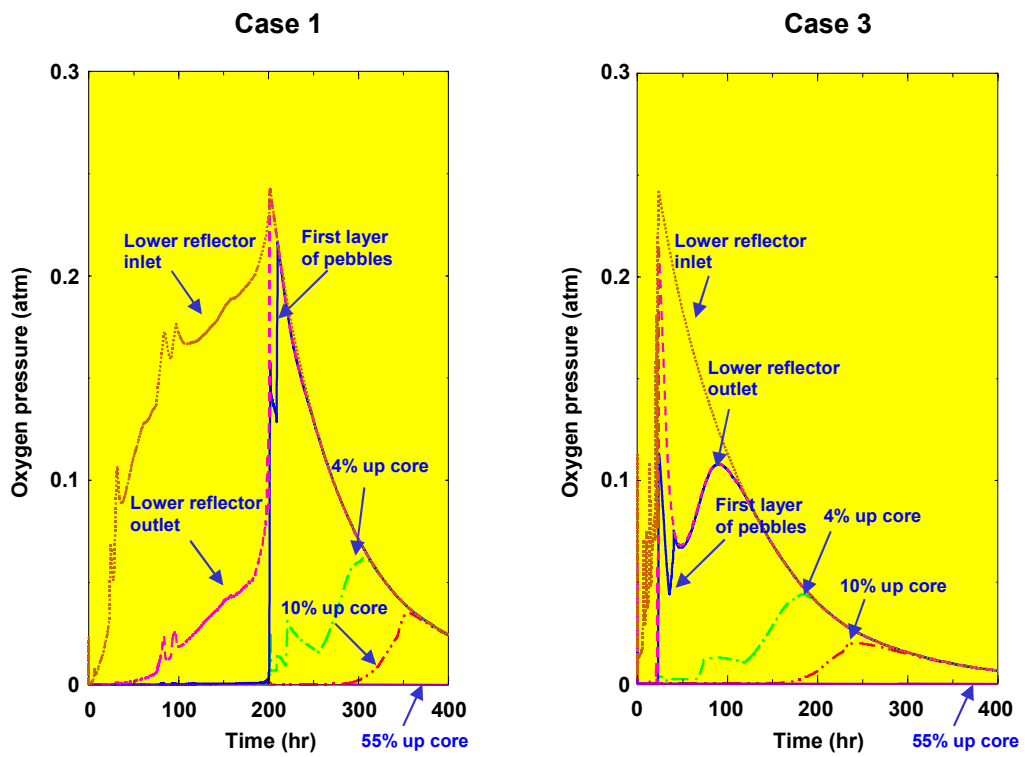


Figure G-17 Oxygen partial pressure history of the core and lower reflector region (Case 3)

layer peaks at 1464°C, which is 145 degrees lower than the peak temperature in the base case. The reason for this is that most of the oxygen is consumed in the upper regions of the lower reflector as is indicated by the oxygen partial pressure curves shown in Figure G-17. The temperatures in the upper core region are essentially the same for Case 3 and the base case because no oxidation occurs in this region of the core. Since more of the oxygen is consumed in the lower reflector region, the maximum partial pressure of oxygen above the first few layer of pebbles is lower than that presented for the base case. From Figure G-17, the partial pressure of oxygen 4% of the way up the core is 0.043 atm compared to 0.060 atm for the base case. No fuel experience temperatures in excess of 1600°C in this case.

### G.8.4 Case 4 - Reduced Core Flow Resistance

Case 4 corresponds to a reduction in the flow resistance in the core by a factor of 10. Temperature and oxygen partial pressure results for this case are presented in Figures 18 and 19. As shown in Figure G-18, the mass flow rate through the core increased from 0.125 kg/s (base case) to 0.214 kg/s as a result of the reduction of the resistance through the core. The onset of natural convection for this case occurs at 220 hours, which is 20 hours later than the base case. This delay in the onset of natural convection is probably due to the localized redistribution of nitrogen in the core. In general the temperature histories are similar to Cases 1 and 2. The pebble temperatures in the first layer peak at 1745°C, which is 134 degrees higher than in the base case but is almost the same as Case 2.

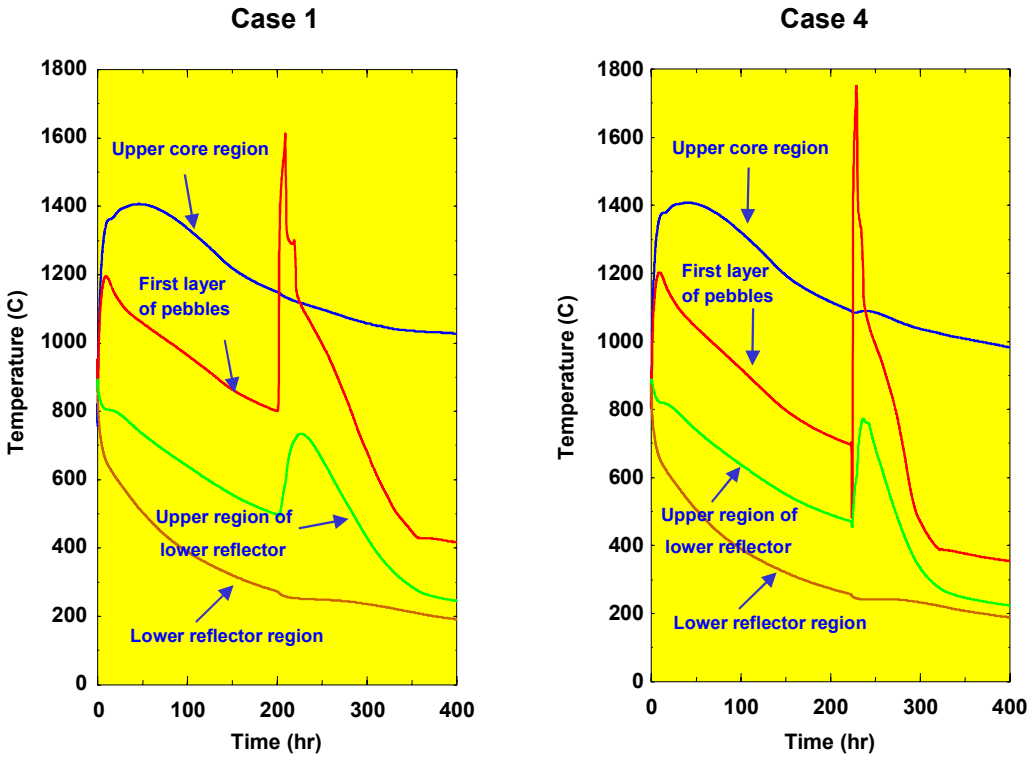


Figure G-18 Temperature history of the core and lower reflector region (Case 4)

This is the result of transporting more oxygen from the containment to the core in roughly the same time period. The pebbles in the bottom layer are above 1600°C for 3.1 hours.

The peak partial pressure of oxygen 4% up the core is 0.064 atm due to the higher transport rate of oxygen to the core. However the maximum temperature in the upper region of the core is the same as for base case thus no oxidation is occurring in this region. As shown in Figure G-19 the oxygen partial pressure 55% of the way up the core is zero. Again only 0.3% of the fueled pebbles experience temperatures in excess of 1600°C.

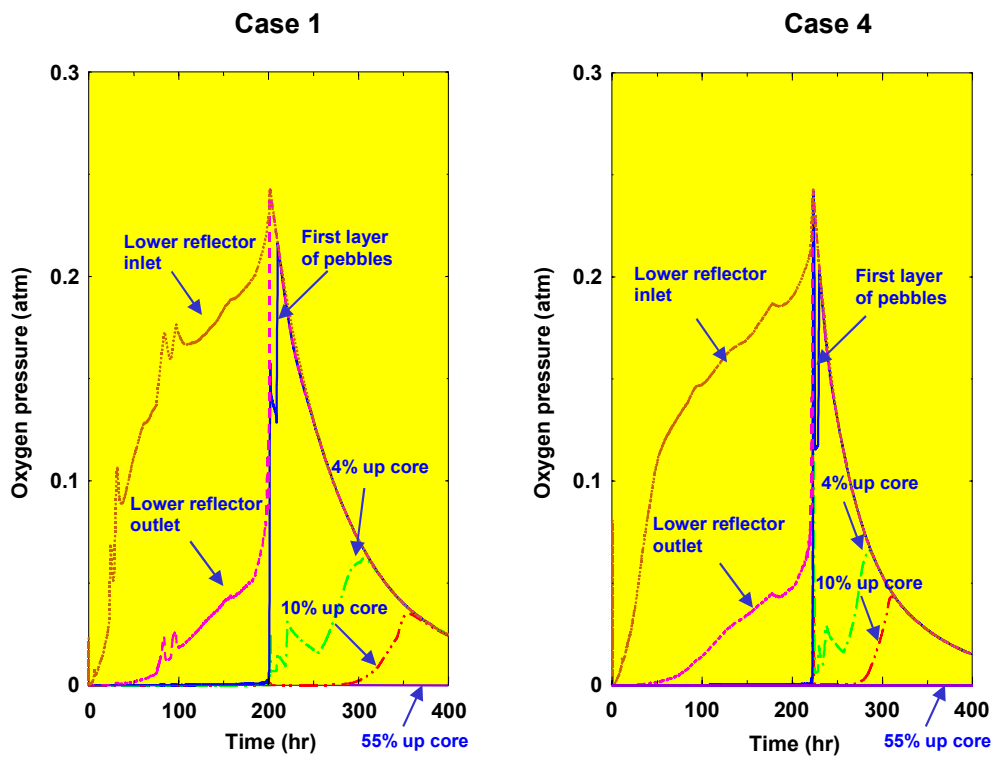


Figure G-19 Oxygen partial pressure history of the core and lower reflector region (Case 4)

### G.8.5 Case 5 - No Oxidation in the Low Reflector Region

Case 5 results correspond to no graphite oxidation in the lower reflector region. Temperature and oxygen partial pressure results for Case 5 are presented in Figures 20 and 21. Viewing Figures 20 and 21 it is seen that the temperature and oxygen partial pressure results for Case 5 are identical to the base case. The results from this case show that the temperature increase of the upper region of the lower reflector is due mainly to conduction and radiation from the lower core region. For the oxidation model used in this study the oxidation rates corresponding to the predicted temperatures in the lower reflector region are too small to support any noticeable oxidation of the graphite in the lower reflector. Oxidation models having higher oxidations rates at lower temperature such as the German data and the INEL 1988 correlation would consumed most of the

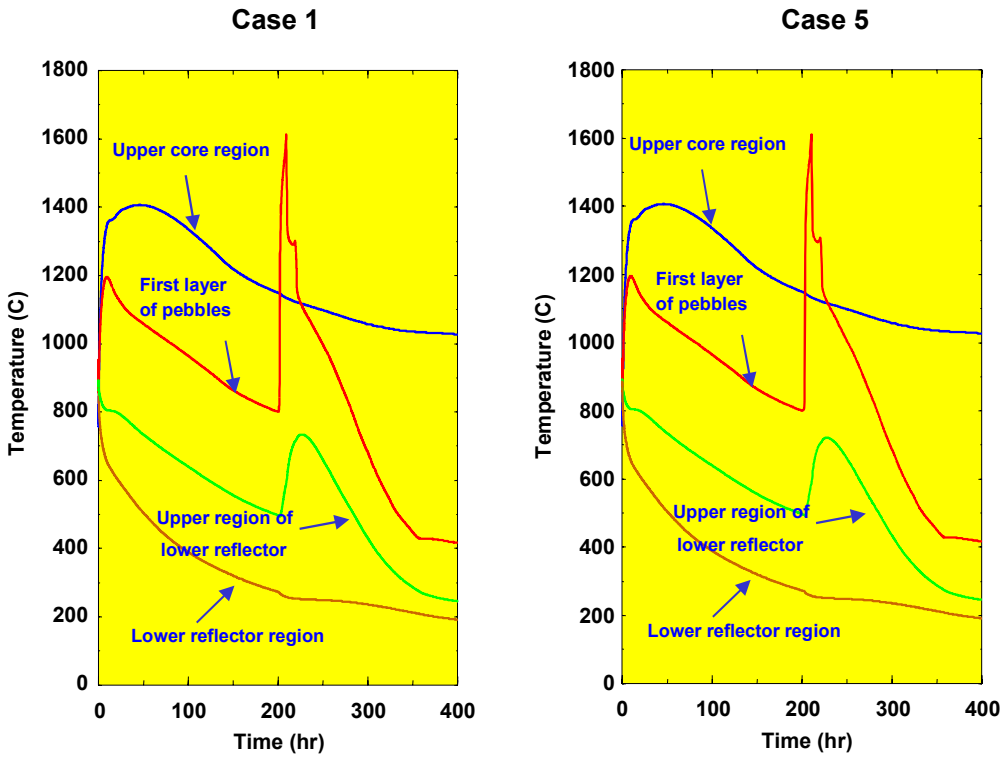


Figure G-20 Temperature history of the core and lower reflector region (Case 5)

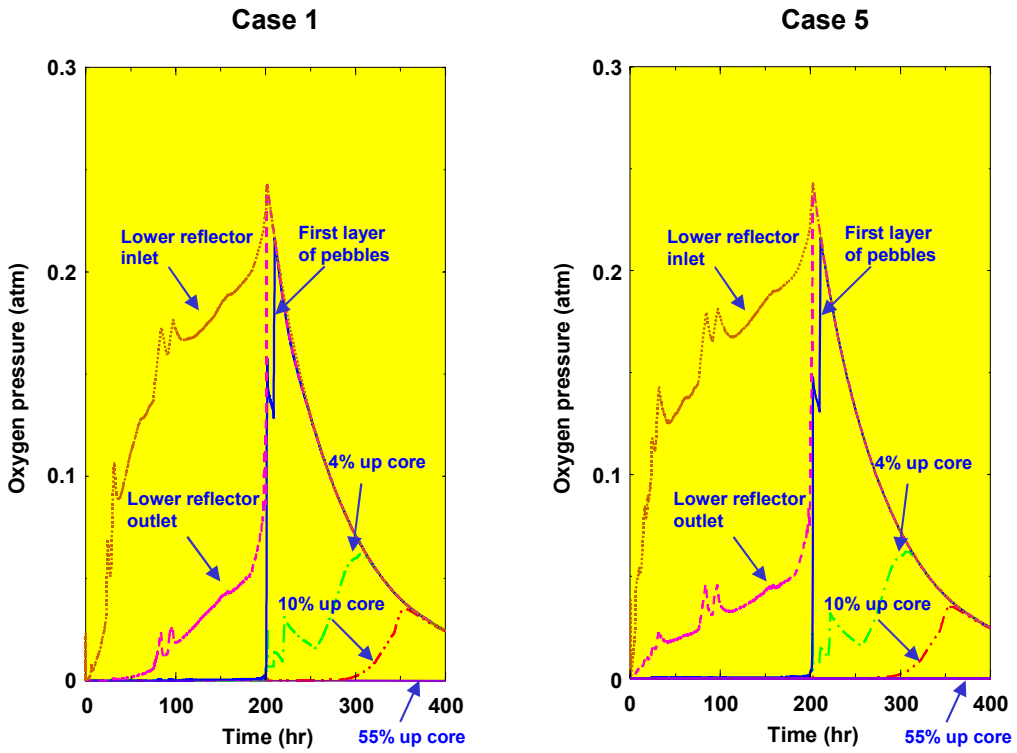


Figure G-21 Oxygen partial pressure history of the core and lower reflector region (Case 5)

oxygen in the air before it reached the pebbles in the core as shown in previous results [G-1]. Again only 0.3% of the fueled pebbles experience temperatures in excess of 1600°C.

### G.8.6 Case 6 - Reduced Side Reflector Thermal Conductivity

Case 6 considered the effect of reducing the thermal conductivity in the side reflectors by 50% on the graphite oxidation in the core and lower reflector regions. The temperature and oxygen partial pressure results for Case 6 are presented in Figures 22 and 23 respectively. Again the results for Case 6 are similar to the result presented for the base

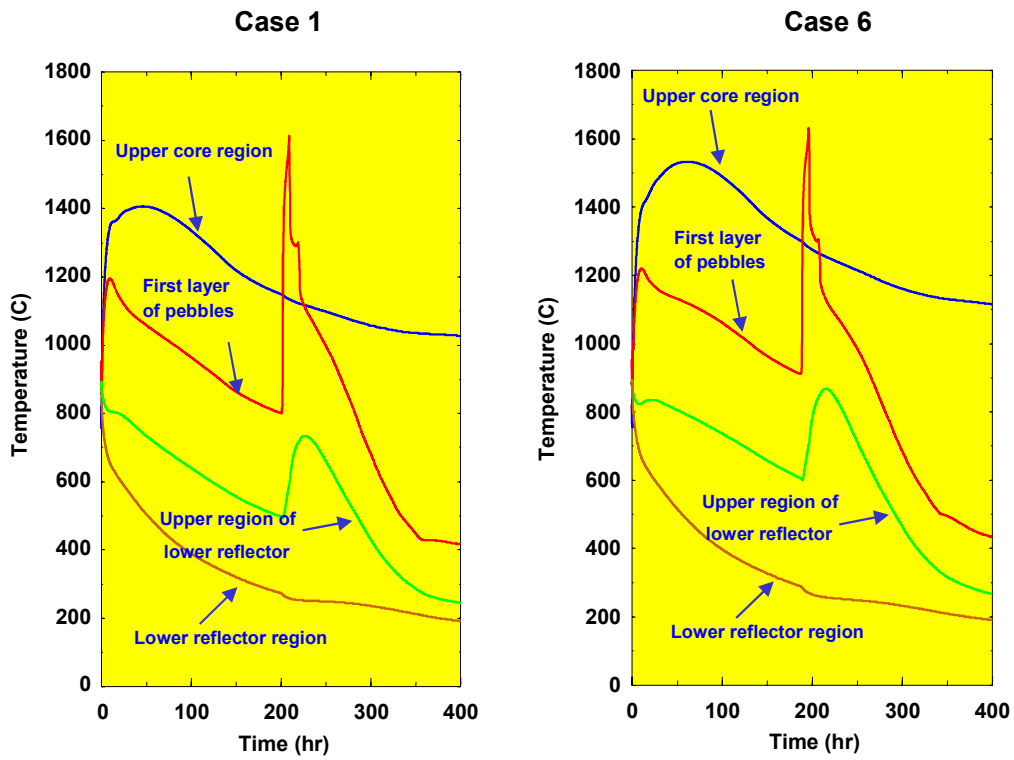


Figure G-22 Temperature history of the core and lower reflector region (Case 6)

case. The temperatures of the pebbles in the bottom layer are at a higher temperature (904°C) compared to (795°C) for the base case at the onset of natural convection resulting in the temperature of the upper region of the lower reflector being higher (600°C) compared to the 500°C value in the base case. This 100°C increase in the temperature of the upper region of the lower reflector results in two orders of magnitude increase in the oxidation rate. Thus, in this case some oxidation occurs in the lower reflector region, which is evident by the fact that the peak temperature in the first layer of pebbles only exceeds the base case by 19°C although it was initially 100°C hotter. Figure G-23 also indicates that oxygen is being consumed in the upper region of the lower reflector. The oxygen partial pressure histories are vary similar to the base case. Here as well only 0.3% of the fuel pebbles experience temperatures in excess of 1600°C.

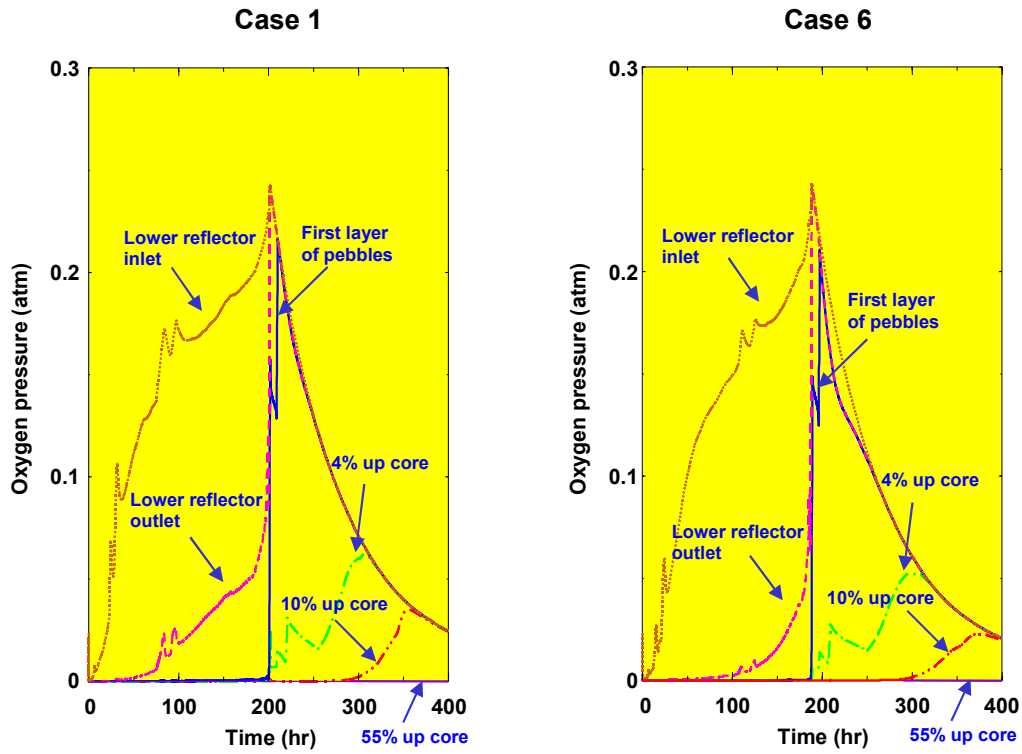


Figure G-23 Oxygen partial pressure history of the core and lower reflector region (Case 6)

### G.8.7 Case 7 - Infinite Containment Volume

Case 7 considers the effect of having an infinite supply of air available for graphite oxidation in the lower reflector and core regions. The temperature and oxygen partial pressure results for Case 7 are presented in Figures 24 and 25 respectively. The major difference between this case and previous cases is that the upper region of the lower reflector experiences substantial oxidation due to the unlimited supply of air. The temperature of the upper region reaches a temperature of 1275°C at 200 hours. The temperature remains at approximately 1275°C for the remainder of transient indicating that the heat generated by oxidation is balanced by the heat removal through the sidewalls of the reactor. The temperature of the bottom layer of pebbles reaches a maximum temperature of 1754°C shortly after the beginning of natural convection (≈ 146 hours). The reflector graphite then cools down to 1060°C where it remains for the remainder of the transients. The temperature of the first layer of pebbles remained above 1600°C for 4.2 hours. The temperature of the upper core region is the same as shown in Case 1 indicating that no oxidation is occurring in the upper regions of the core at least out to 400 hours.

From Figure G-25 it is seen that the partial pressure in the bottom layer of pebbles is the same as in the upper region of the lower reflector. This indicates that all the graphite in the bottom layer of pebbles is consumed by 180 hours. The partial pressure of oxygen 4% of the way up the core (CV(008)) increases to the same level as in the upper region of

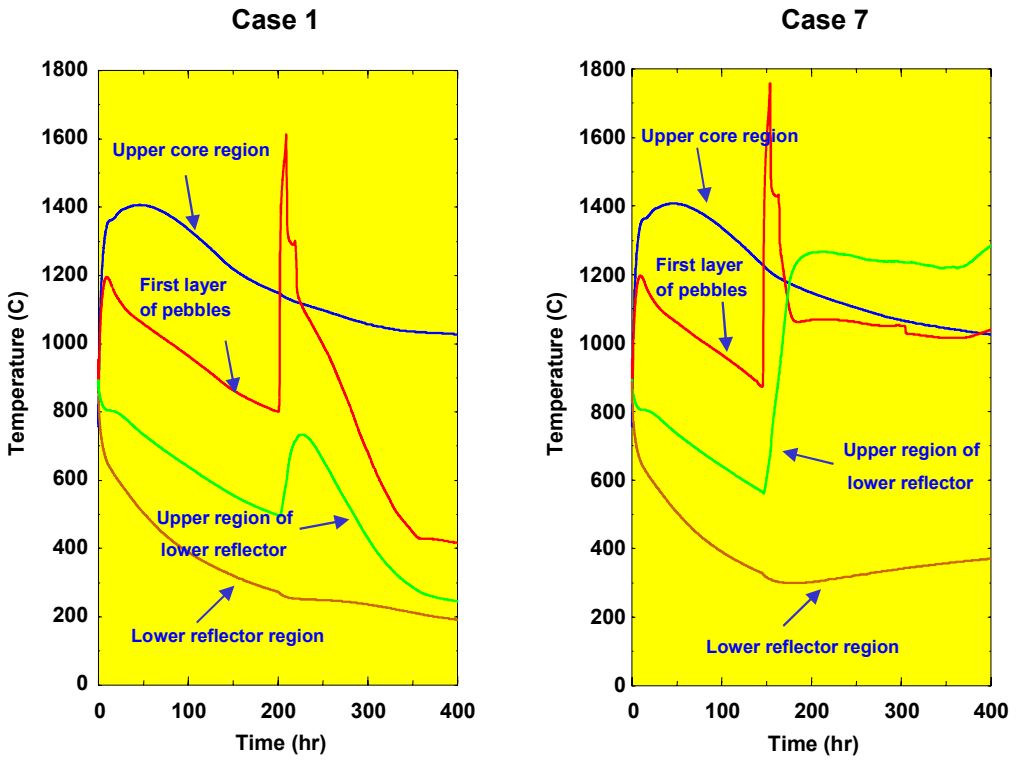


Figure G-24 Temperature history of the core and lower reflector region (Case 7)

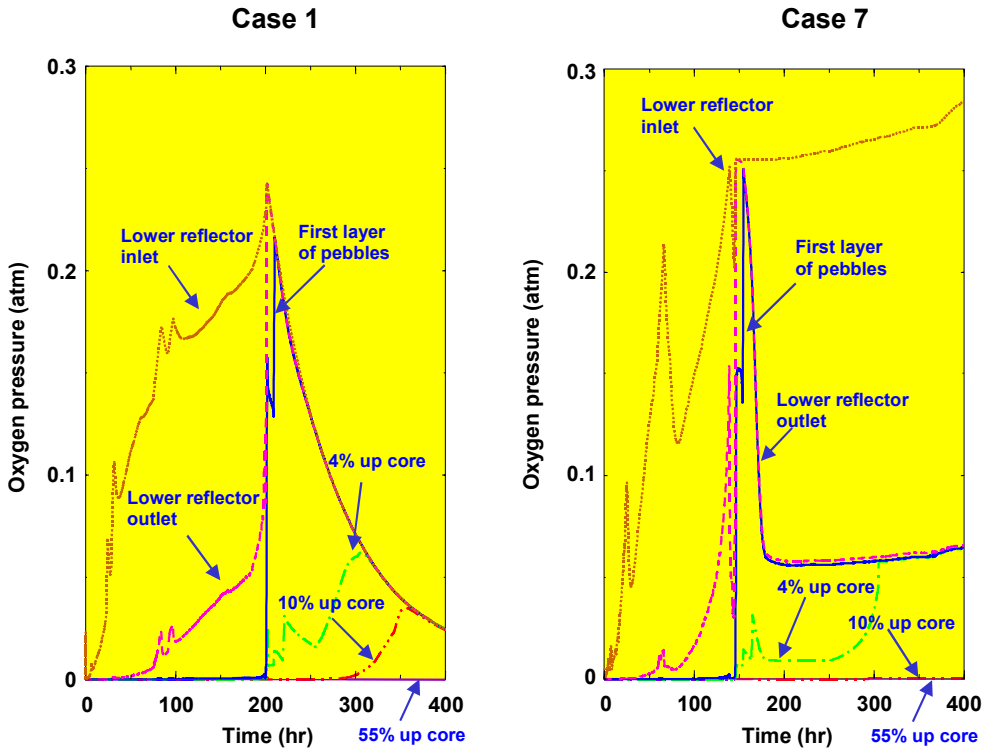


Figure G-25 Oxygen partial pressure history of the core and lower reflector region (Case 7)

the lower reflector at approximately 300 hours into the transient which indicates that the graphite in the pebbles in CV(008) has also been consumed by oxidation. The results presented in Figure G-25 indicates that no oxidation (at least out to 400 hours) is occurring above CV(014) which is located approximately 10% above the bottom of the core. At the end of 400 hours 1.5% of the fueled pebbles have been consumed.

### G.8.8 Case 8 – All Factors Combined

Case 8 consists of a combination of all of the factors in the seven previous cases. This case is therefore considered to be extremely conservative or even excessively conservative. The temperature and partial pressure results for this case are presented in Figures 26 and 27 respectively. As in Case 3 the beginning of natural convection occurs at 22 hours. The temperature of the bottom layer of pebbles peaks at 1986°C and remains above 1600°C for 33 hours. However, as indicated in Figure G-27, the graphite in the bottom layer of pebbles is fully consumed by 26 hours (the partial pressure of oxygen increases to 0.2 atm which is the same as in the containment). The temperature plot of the first layer of pebbles shows the temperature continuing to decrease due to the assumption that a small radius of the pebble (r = 0.005m) cannot be oxidized.

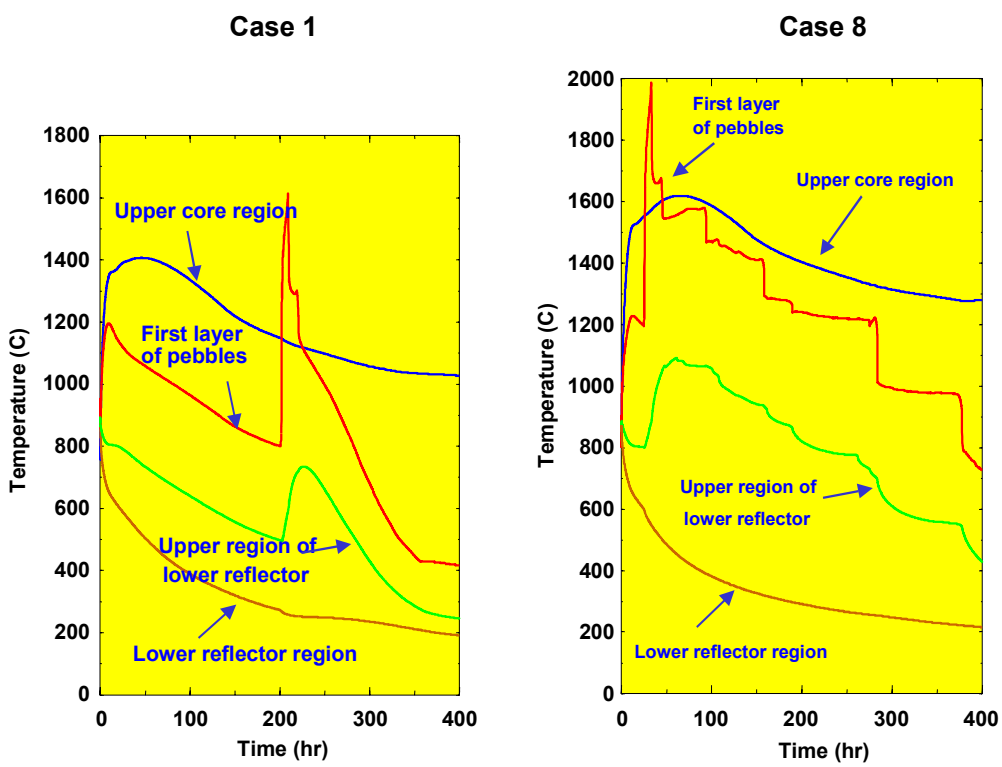


Figure G-26 Temperature history of the core and lower reflector region (Case 8)

This was necessary to eliminate any division by zero when the radius of the pebble goes to zero. The partial pressure results presented in Figure G-27 show that the pebbles in the layer 4% of the way up the core are consumed by 158 hours and the pebbles 10% up the core are consumed by

378 hours. This case indicates extremely severe graphite oxidation would be predicted if air ingress into the core occurs at very high core temperatures.

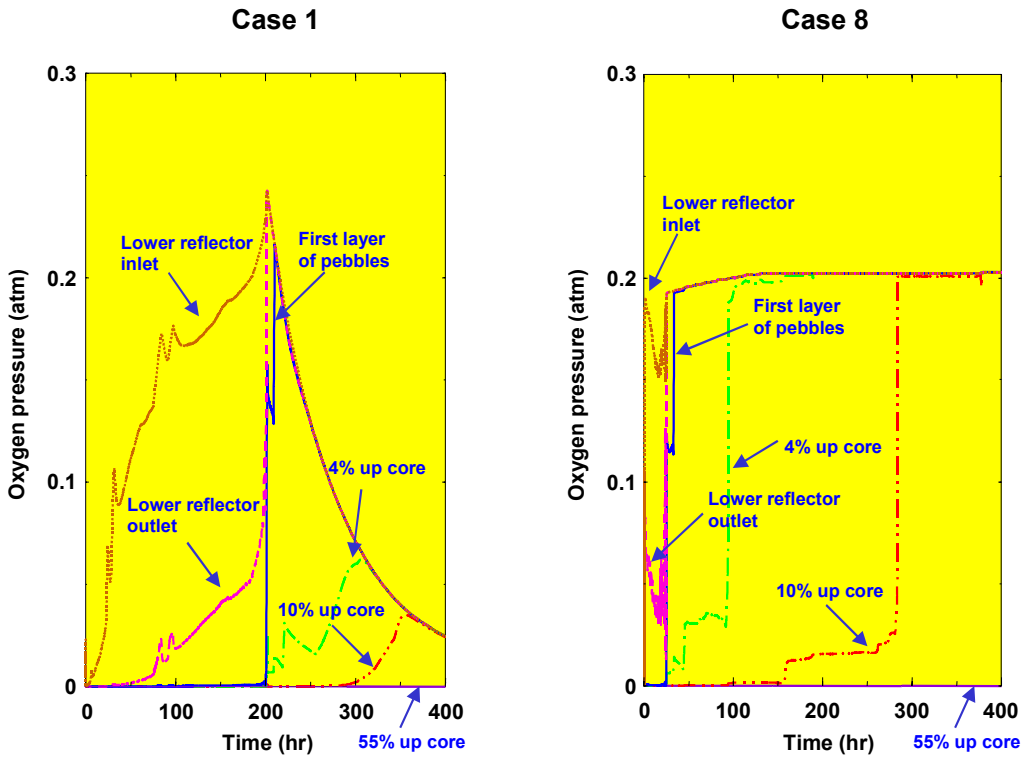


Figure G-27 Oxygen partial pressure history of the core and lower reflector region (Case 8)

The final figure present is Figure G-28, which shows the mass flow rates through the core for several of the sensitivity cases. The mass flow rates range from 0.1 kg/s to 0.125 kg/s except for the low core resistance case (Case 4) where the mass flow rate peaked at 0.22 kg/s. The onset of natural convection ranged from 22 hours for the upper head leak case to 225 hours for the low core flow resistance case.

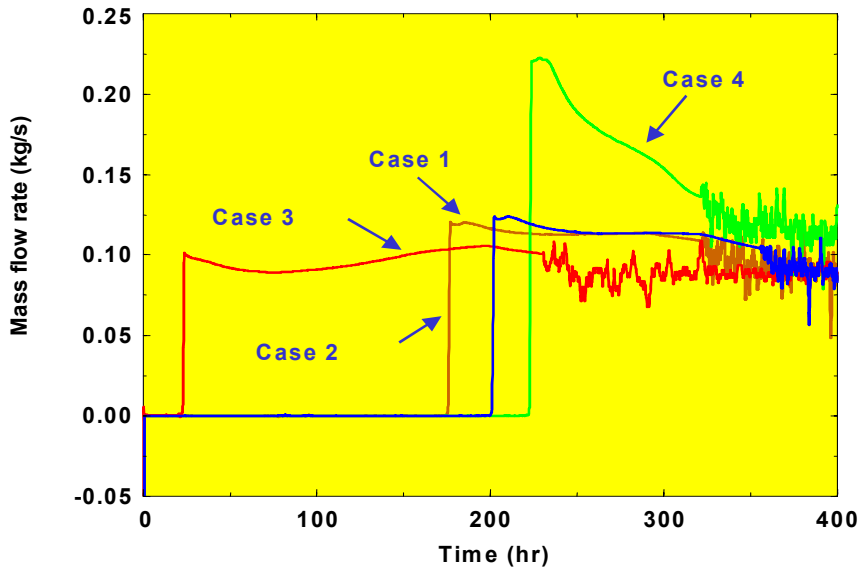

Figure G-28 Mass flow rate for Cases 1, 2, 3, and 4

## G.9 Conclusions

The results of the scoping studies showed a remarkably consistent picture of the oxidation event:

1. Following depressurization, there is an incubation time associated with molecular diffusion of oxygen into the reactor. The incubation time ranged from 22 hours to 220 hours depending on assumptions related to the hydraulics of the system.

2. Very little oxidation occurs in the lower reflector region except for the upper head leak case (Case 3), the infinite containment case (Case 7), and Case 8 (combined case). Overall oxidation is limited to the lower 10% of the core. Partial pressures of oxygen in these regions range from 0.05 to 0.24 atm. Little or no oxidation occurs in the upper core region because of complete consumption of air with the exception of the case of infinite availability of air.

3. The amount of fuel at risk in the oxidation transient is limited. In all but the worse case scenario, the oxidized fuel pebbles experience temperature between 1600 and 1750°C for only 0.5 to 5 hours depending on the case.

4. The destruction of pebble matrix material and higher than normal temperatures allows the migration of fission products that were released during normal operation and the convection flow can act as a mechanism to transport these fission products out of the core. However, the potential source term is likely to be bounded by $\approx 10^{-4}$ normal operating fuel failure fraction since core temperatures do not exceed 1600°C for long periods of time.

## G.10 References


G-1. Moore, R. L., C. H. Oh, B. J. Merrill, D. A. Petti, "Studies on Air Ingress for Pebble Bed Reactors," Proceedings of HTR 2002, 1st International Topical Meeting on High Temperature Reactor Technology (HTR), Petten, Netherlands, April 22-24, 2002.

G-2. Gauntt, R. O., R. K Cole, C. M. Erickson, R. G. Gido, R. D. Gasser, S. B. Rodriguez, and M. F. Young, "MELCOR Computer Code Manuals," NUREG/CR-6119, Vol 1 and 2, Rev. 2, SAND2000-2417, 2000.

G-3. Merrill, B. J., R. L. Moore, S. T. Polkinghorne, and D. A. Petti, "Modifications to the MELCOR code for application in fusion accident analyses, "*Fusion Engineering and Design*, **51-52**, (2000) pp555-563.

G-4. Niessen, H, and S. Ball (editors), Heat Transport and Afterheat Removal for Gas Cooled Reactors Under Accident Conditions, International Atomic Energy Administration, IAEA-TECDOC-1163.

G-5. Zehner, P., and E. U. Schlünder, "Thermal Conductivity of Granular Material at Moderate Temperatures," *Chemie-Ingr-Tech*, 42, pp933-941, 1970. In German.

G-6. Breitbach, G., and H. Barthels, "The Radiant Heat Transfer in the HTR Core After Failure of the Afterheat Removal Systems," *Nuclear Technology*, 49, pp392-399, August 1980.

G-7. Prasad, V., N. Kladas, A. Bandyopadhaya and Q. Tian, "Evaluation of Correlations for Stagnant Thermal Conductivity of Liquid-Saturated Porous Beds of Spheres," *International Journal of Heat and Mass Transfer*, 32, pp1783-1796.

G-8. Mathcad 11 User's Guide, Mathsoft Engineering & Education, Inc. Cambridge, MA.

G-9. H. C. No, "PBR System Simulation Code for Depressurization Accident Analysis in a Modular Pebble Bed Reactor," Massachusetts Institute of Technology, Un-Published.

G-10. Savage, M. G., "A One-Dimensional Modeling of Radial Heat Removal During Depressurized Heatup Transients in Modular Pebble-Bed and Prismatic High Temperature Gas-Cooled Reactors," Oak Ridge National Laboratory, ORNL/TM-9215, July 1984.

G-11. Terry, W. K., H. D. Gougar, and A. M. Ougouag, "Deterministic Methods for Fuel-Cycle Analysis in Pebble-Bed Reactors," Trans. Am. Nucl. Soc. 83, 2000, pp. 273-279.

G-12. Terry, W. K., H. D. Gougar, and A. M. Ougouag, "Direct Deterministic Method for Neutronic Analysis and Computation of Asymptotic Burnup Distribution in a Recirculating Pebble-Bed Reactor," *Annals of Nucl. Energy* 29, 2002, pp. 1345-1364.

G-13. Wicke, E., Fifth Symposium on Combustion, Reinhold, New York, 1955.

G-14. Rossberg, M., and E. Wicke, *Chem.-Ingr.-Tech*. 28, 181 1956.

G-15. O'brien, M. H., B. J. Merrill and S. N. Ugaki, Combustion Testing and Thermal Modeling of Proposed CIT Graphite Tile Materials, Idaho National Engineering Laboratory, EGG-FSP-8255, 1988.

G-16. Marshall, T. D., R. J. Pawelko, R. A. Anderl, G. R. Smolik, B. J. Merrill, and R. L. Moore, Air Chemical Reactivity Measurements of Carbon Fiber Composite NB31, Idaho National Engineering and Environmental Laboratory, INEEL/EXT-02-00745, May 2002.

G-17. Schroeder, B., W. Schenk, Z. Alkan, and R. Conrad, Ceramic Coatings for HTR Graphitic Structures – Tests and Experiments with SiC-Coated Graphitic Specimens, OECD/NEA First Information Exchange Meeting on Survey on Basic Studies in the Field of High Temperature Engineering (including Safety Studies), Paris, France, September 1999, pp. 27-29.

G-18. MELCOR Computer Code Manuals, "Thermal Hydraulic (CVH and FL) Packages", NUREG/CR-6119, Vol. 2, CVH/FL-RM-17, May 2000.

G-19. MELCOR Computer Code Manuals, "Material Properties (MP) Package", NUREG/CR-6119, Vol. 2, MP-RM-55, May 2000.

G-20. Takeda, T., and M. Hishida, "Studies on diffusion and natural convection of two-component gases," *Nuclear Engineering and Design*, 135, 1992, pp. 341-354.

G-21. Th. Schaaf, Th., W. Frohling, H. Hohn and S. Struth, "The NACOK experimental facility for investigation an air ingress into the core of a high temperature reactor," *Kerntechnik*, 63, 3, 1998, pp. 107-112.